TUDelft

Delft University of Technology

Tidal Energy Assessment | North Sea Tidal Database

Alday Gonzalez, M.F.; Lavidas, G.

Publication date
2022
Document Version
Final published version
Citation (APA)
Alday Gonzalez, M. F., & Lavidas, G. (2022). *Tidal Energy Assessment | North Sea Tidal Database*. TU Delft - Faculty of Civil Engineering and Geosciences.

Important note
To cite this publication, please use the final published version (if applicable).
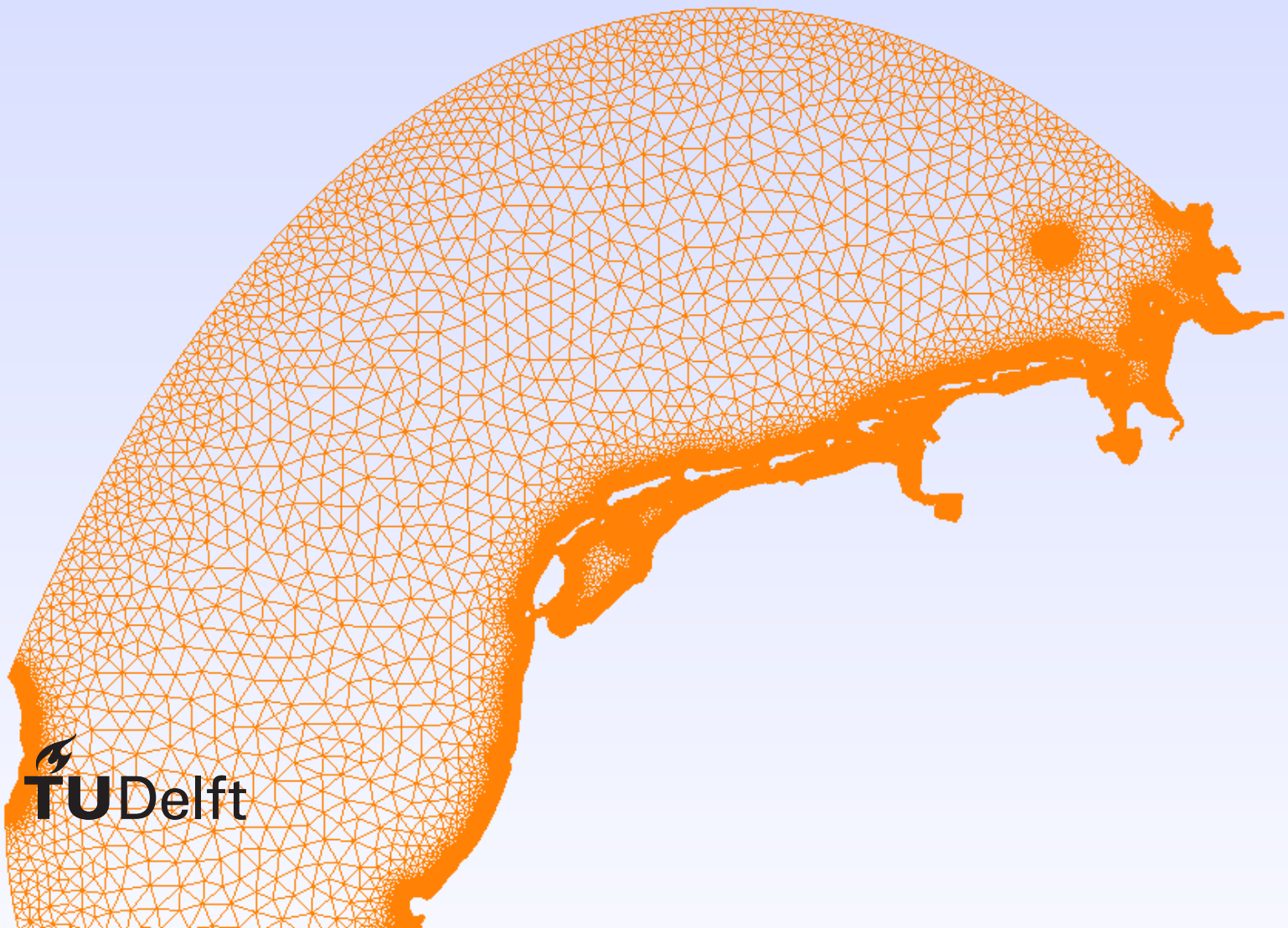Please check the document version above.

Dutch-WATERS

Dutch-Wave And Tidal Energy ResourceS

Tidal Energy Assessment | North Sea Tidal Database

Marine Renewable Energies Lab

TUDelft

Dutch-WATERS
Dutch-**W**ave **A**nd **T**idal **E**nergy Resource**S**

by

Marine Renewable Energies Lab (MREL)
Offshore Engineering (OE) Group
Hydraulic Engineering (HE) Department
Faculty of Civil Engineering & Geosciences (CEG)

Project duration: January 1, 2022 – January 1, 2023
Authors: Dr Matias Gonzalez Alday   TU Delft
                    Dr George Lavidas   TU Delft

An electronic version of this report is available at
http://repository.tudelft.nl/ & at
www.tudelft.nl/ceg/mrel.

ŤUDelft

Contents

1

Dutch-Wave And Tidal Energy ResourceS

The Netherlands with its long coastline and strong offshore expertise is optimally suited for implementing renewable offshore marine energy solutions. To complement and support the energy transition driven by wind and solar, also wave and tidal resources should be exploited. A quantification of the role of these resources in the Dutch energy system requires an assessment of the available wave and tidal resources. Dutch-WATERS generates wave and tidal datasets with state-of-the-art modelling, which are verified with in-situ measurements.

Dutch-WATERS primarily contributes to mission F: The Netherlands as the best-protected and most viable delta in the world, with timely future-proof measures implemented at a manageable cost. Within this mission, the main focus is on MMIP F4: Energie uit water. The objective of MMIP F4 is to use water as a source for renewable energy. Both wave and tidal stream energy are named in this MMIP. Dutch-WATERS develops calibrated numerical wave and tidal models to support the development of wave energy, tidal barrages, small hydro-electric and tidal stream technologies, ultimately, enhancing the metocean information for the North Sea. The interaction with Dutch companies will allow to link this metocean data directly to potential electricity production capabilities. Both, the resource assessments as well as the production data also connects to MMIP F3, Nederland digitaal waterland, by providing direct input to a digital twin of the Dutch North Sea to improve human activities.

Secondary, benefits from the Dutch-WATERS generated resource assessment are of added value for future analysis on coastal protection (MMIP F2, Aanpassen aan versnelde zeespiegelstijging) and a more sustainable North Sea (MMIP E1). In MMIP F2 the resource assessment can provide insight into increasing tidal differences and wave heights, which can contribute to a safer and more future-proof delta. In MMIP E1 the data can provide new insights necessary for a sustainable balance between ecological capacity and water management versus renewable energy, food, fishing and other economic activities. Especially the development of marine spatial planning for the Dutch North Sea can greatly benefit from assessing wave and tidal resources.

Besides the contributions to three MMIPs linked to TKI Deltatechnology, Dutch-WATERS also connects to the MMIP 1 offshore renewable energy, which is led by TKI Wind op Zee (Topsector Energy). This MMIP focuses on enabling the required scale-up for offshore renewable energy, especially offshore wind energy, and also other forms of offshore energy in the longer term. The project specifically addresses the sub-themes of energy system integration and environmental integration within this MMIP. However, the primary focus of this TKI is on offshore wind, therefore the TKI Deltatechnology was chosen as the best suited for the Dutch-WATERS project.

2

Tidal Modelling

Unlike wind, one of the key-points that makes the tidal energy resource attractive for electricity generation, is its predictability. Although, there would be a locally intermittent production, characteristic of a given site's tidal cycle, this effect can be mitigated with a carefully designed layout of energy converters, taking advantage of the tidal phase lag along the coast. In areas of relatively shallow water depths (<20 m) and/or complex coastlines configurations, bathymetry features become more important as they can significantly modify the hydrodynamic field, potentially inducing areas of high velocities (tidal jets) even when tidal elevation's amplitude is not necessarily "extreme" as found in some locations within the English Channel or in the UK.

Here we make a first effort to characterize the sea surface elevation changes and current velocities pattern induced by astronomical tides along the Dutch coast, with a high resolution hydrodynamic model. In the following sections, specifications of the implemented model formulations, numerical scheme, modelled domain and boundary conditions are presented.

2.1. The THETIS model

THETIS [13] is an open source python-based ocean and coastal modelling suit, that works with the Firedrake finite element framework [19] and the Portable, Extensible Toolkit for Scientific Computation [PETSc; 3, 4] to solve Partial Differential Equations (PDE) systems.

Astronomical tides are long barotropic waves, given their nature and the purpose of the present study, it is suitable to represent the induced motions in the water column as 2-dimensional, neglecting the vertical velocities component. In our implementation of THETIS we solve the Nonlinear Shallow Water Equations (NLSWE) over a finite elements unstructured grid (mesh). The system is solved in space and time respectively with a CG-type [11] and a 2-stage 2nd order L-stable Diagonally Implicit Runge Kutta [DIRK22; 1] implicit method.

In the following sections we provide further details on the solved equations, mesh construction, numerical choices and forcing fields considered.

2.1.1. Nonlinear shallow water equations

The depth averaged shallow water equations as implemented in THETIS are described as follows:

$$\frac{\partial \eta}{\partial t} + \nabla \cdot (H\overline{u}) = 0 \tag{2.1}$$

$$\frac{\partial \overline{u}}{\partial t} + \overline{u} \cdot \nabla \overline{u} + f e_z \wedge \overline{u} + g\nabla \eta + \nabla\left(\frac{\rho_a}{\rho_0}\right) + g\frac{1}{H}\int_{-h}^{\eta} \nabla r \, dz = \nabla \cdot \left(\nu_h(\nabla \overline{u} + (\nabla \overline{u})^T)\right) + \frac{\nu_h \nabla(H)}{H} \cdot (\nabla \overline{u} + (\nabla \overline{u})^T) \tag{2.2}$$

with

$$r = \frac{1}{\rho_0}\int_z^{\eta} \rho' \, d\zeta \tag{2.3}$$

and

$$H = \eta + h \tag{2.4}$$

The state variables are the water elevation η and the depth averaged velocity vector $\overline{u}$. Then eq. 2.1 is the non-conservative form of the free surface, eq. 2.2 is the expression for the non-conservative momentum, where eq. 2.3 denotes the baroclinic head. In particular for our application with purely baroclinic components, eq. 2.3 and the internal pressure gradient are omitted. Finally, the total water column depth is given by eq. 2.4.

Notice that we haven't included any external pressure gradient term as we are only considering the effect of astronomical tides.

2.1.2. Mesh construction and domain extension

The two-dimensional unstructured grid was generated using the qmesh mesh generator [2], integrating coastlines from OpenStreetMaps [OSM; 16] and bathymetry data from the EMODnet digital elevation model [version 2020; 23] with a gridded resolution of ~115 m. Before the mesh generation, the variable resolution from OSM polygons was homogenized along the Dutch coast at a maximum resolution of ~500 m applying decreasing resolution along the English Channel, the UK and the Atlantic coast of Europe. All small islands outside the area of interest and in deep water depths were not considered to optimize modelling time and CPU usage.

Both, bathymetry and coastlines data were re-projected from geographical coordinates to WGS84, UTM zone 31 North. Additionally, bathymetry's vertical datum was transformed from Lowest Astronomical Tide (LAT) to Mean Sea Level (MSL) with the M_2, S_2, N_2, K_1 and O_1 tidal harmonics' amplitudes from the Ifremer's Tidal Atlas [18] using the following approximation:

$$\text{LAT}_{(x,y)} = \quad \text{Zo}_{(x,y)} - \sum (\text{A}_{i(x,y)}) \tag{2.5}$$

where $\text{LAT}_{(x,y)}$ is the estimated LAT datum at a given location (x,y) and $\text{A}_{i(x,y)}$ is the amplitude from the i-th considered harmonic for datum correction.

The modelled domain is extended to deep waters off the European coastal shelf in most of its extension along the North Atlantic. This is done to facilitate numerical stability and allow the tidal waves' interaction with the main bathymetric features as it propagates towards the dutch coast. To control the mesh elements size distribution, mainly 2 restrictions or metrics where taken into account. First a minimum element size relate to wave propagation celerity in shallow waters, which is proportional to the local depth $C = \sqrt{gH}$, considering that N = 3 mesh elements are required to capture the minimum tidal wave length as proposed in Lambrechts et al. [15]. The second metric is related to the minimum element side length desired at identified boundaries (e.g. open boundaries, continental or islands coastlines) and how they grow as function to the distance from each given boundary. A total of 6 boundaries IDs where defined to progressively increase the mesh elements' size towards the open boundary in deep waters (ID = 2000) and still preserve relevant coastlines and bathymetry features. Along the Dutch coast (boundary ID = 1000) we defined a minimum element side length of 500 m, this restriction is only relaxed 4 km off the shore to ensure a high resolution band along the area of interest (see Fig. 2.1).

Once the mesh is defined, the input bathymetry is interpolated into the mesh's nodes in THETIS, in this case using bi-linear interpolation (see Fig. 2.2).
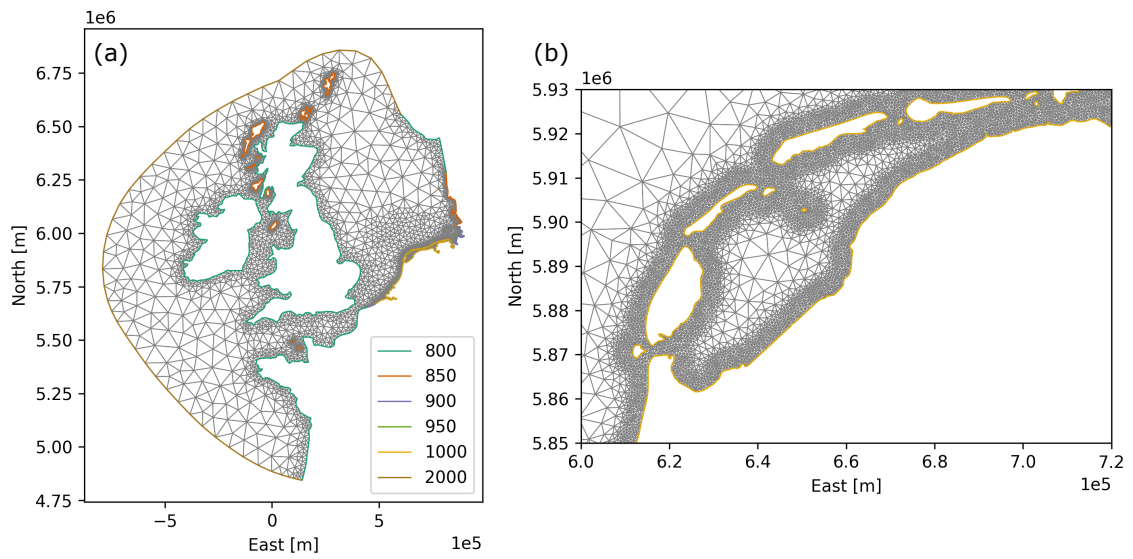
Figure 2.1: (a) Mesh elements distribution in full domain (b) Mesh elements detail along part of the Dutch coast. ID = 2000 is the open ocean boundary where boundary conditions are prescribed. ID = 1000 is the Dutch coast boundary with maximum resolution. ID's 950 to 800 are used to help reducing mesh elements resolution towards the open boundary.
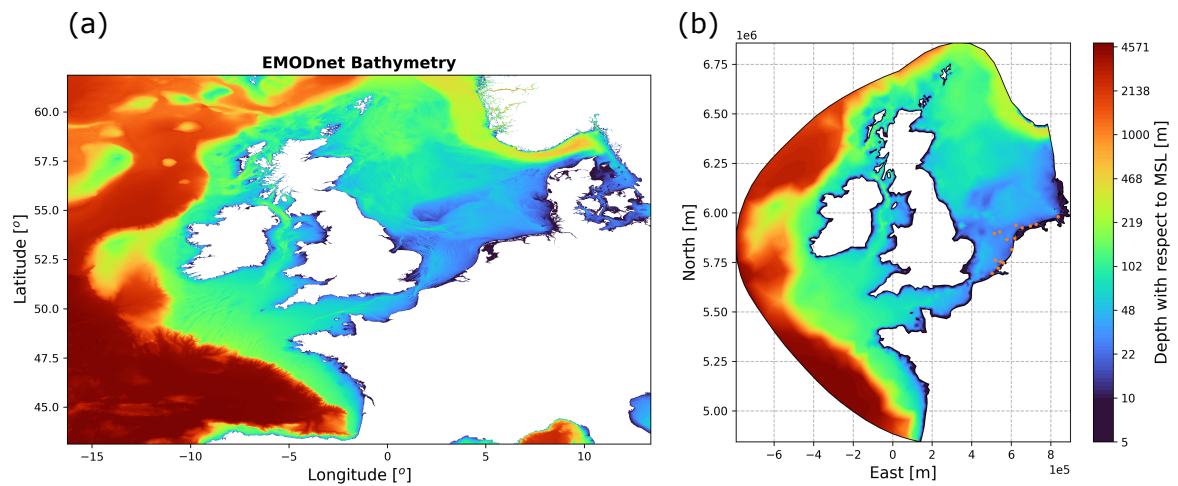

Figure 2.2: (a) EMODnet bathymetry DEM on its original projection. (b) Bathymetry interpolated into mesh nodes. Orange points in (b) show the location of the tide gauges used for validation.

2.1.3. Numerical choices

Even though the implicit time solving scheme is unconditionally stable, a maximum time step of 360 s was defined based on CFL stability conditions for explicit numerical methods [6]. This is done to prevent the simulation of unrealistic levels and/or current intensities values in those regions of the modelled domain with high resolution. In the same line, a minimum depth threshold of 7 m is applied in the model, which means that shallower depths are internally set to this minimum depth. Finally, an ad hoc homogeneous Manning friction coefficient of 0.0255 $m^{1/3}s^{-1}$ was set for the complete domain. This approach should be re-visited in further efforts to help reduce the spatial distribution of random errors [e.g. 14].

Output of the depth averaged velocities components u and v, and water elevation is requested each 30 minutes.

2.1.4. Forcing

The model is forced with tidal levels at the open ocean boundary (Fig. 2.1a). The tidal levels are generated based on the harmonics (amplitudes and phases) taken from the OSU TPXO global barotropic tide model [TPXO9v5a; 7]. A total of 11 harmonics are included: Q1, O1, P1, K1, N2, M2, S2, K2, M3, M4, and S1. The amplitudes and phases with originally 1/6° grid resolution are interpolated along the nodes of the open boundary. The placement of the open boundary in deep waters (outside the coastal shelf) was also defined taking into account the small intensities of tidal currents in the area, making it adequate to force just with tidal levels and letting the velocities develop inside the domain.

To force the model, a spin-up time of 15 days was considered with linearly increasing amplitudes until reaching full forcing. After these 15 days, 2 extra days are included with boundary forcing with its full amplitudes before using the modelled output data.

2.2. Preliminary validation

At this stage, validation of the model is performed for elevations only. A total of 13 locations distributed along the Dutch coast were selected to compare against in-situ measurements from tide gauges (TG) obtained from the CMEMS in Situ TAC platform [22]. The year 2016 was selected due to the large amount of simultaneous data available at different locations.

The following performance parameters where used to assess the accuracy of the simulations:

$$\text{ABIAS} \quad = \quad \frac{1}{N}\sum(|X_{\text{mod}}| - |X_{\text{obs}}|) \tag{2.6}$$

$$\text{RMSD} \quad = \quad \sqrt{\frac{\sum(X_{\text{mod}} - X_{\text{obs}})^2}{N}} \tag{2.7}$$

$$\text{NRMSD} \quad = \quad \sqrt{\frac{\sum(X_{\text{mod}} - X_{\text{obs}})^2}{\sum X_{\text{obs}}^2}} \tag{2.8}$$

$$\text{CORR} \quad = \quad \frac{\sum(X_{\text{mod}} - \overline{X_{\text{mod}}})(X_{\text{obs}} - \overline{X_{\text{obs}}})}{\sqrt{\sum(X_{\text{mod}} - \overline{X_{\text{mod}}})^2}\sqrt{\sum(X_{\text{obs}} - \overline{X_{\text{obs}}})^2}} \tag{2.9}$$

where ABIAS is the bias of the absolute value of sea surface elevations. RMSD are the Root Mean squared Differences and NRMSD the Normalized Root Mean Squared Differences. Within these expressions X_{mod} are the modelled tidal elevations and X_{obs} the reference value from measurements (tide gauges).

Analysis of the model's results performance was done for the complete year 2016. To identify potential seasonal effects of other forcing not included in our Thetis implementation, we defined time windows of 2 months to compute ABIAS, RMSD, NRMSD and CORR. A briefing of the validation results for all locations is presented in table 2.1 for winter and summer months. From Fig. 2.3 to 2.5 we present a selection of 3 locations and 3 different time windows within the selected year to visualize the presence of seasonal changes.

The largest RMSD and NRMSD a lower CORR values are found for the January-February period at all analyzed locations (table 2.1) . On the other hand, for the summer months (July-August) we found the smallest error values as well as the higher correlations, typically over 93 %. We suspect that these seasonal changes are related to the presence of a non-astronomical component in the TG records that is more significant during winter. The occurrence of "events" where differences between modelled and measured elevations are largest, fall within the same days at different locations. This suggest the influence of low atmospheric pressure and

potentially energetic sea states in the recorded time series. For example, from 1 to 4 of February (see Fig. 2.3a to Fig. 2.5a), data from the ECMWF ERA5 atmospheric re-analyses [10] shows average wind intensities of 15.8 ms^{-1} and wave heights (combined swell and sea) of ~ 4.5 m close to the Dutch coast. The influence of other forcing over the currents profile should be further analyzed to assess its impact in the resource estimation.

Since we are forcing the model only with astronomical tides, it makes sense to compare the simulated results with TG data from those months where the astronomical tide signal is dominant (e.g. Fig. 2.3b,c to Fig. 2.5b,c). As mentioned earlier, the high "model-TG" elevation correlations above 0.9 and reduced ABIAS proves a good representation of the tidal amplitudes along Dutch waters. Even though there is a noticeable reduction of the NRMSD between July to September, in some places it can still be > 30 %. These differences are due to slight relative phase shifts between the modelled tidal wave and the TG data. This effect could be attributed to the mooring system of the instruments, inaccuracies in the phase values from the TPXO model constituents used along the boundary or the use of a homogeneous bottom friction coefficient in the modelled domain.

TG Location Name	Longitude [°]	Latitude [°]	Time period	ABIAS [m]	RMSD [m]	NRMSD [%]	CORR (ρ_{Pearson})
AlteWeser	8.1275	53.8633	Jan–Feb	-0.11	0.48	44.04	0.899
			Jul–Aug	-0.085	0.209	20.111	0.983
DenHelder	4.75	52.97	Jan–Feb	-0.77	0.346	57.409	0.819
			Jul–Aug	-0.023	0.161	31.051	0.951
Europlatform	3.28	52.0	Jan–Feb	-0.135	0.309	48.992	0.882
			Jul–Aug	-0.107	0.207	35.447	0.945
Haringvliet10	3.86	51.864	Jan–Feb	-0.138	0.343	43.273	0.909
			Jul–Aug	-0.106	0.232	31.45	0.954
Huibertgat	6.4	53.57	Jan–Feb	-0.089	0.397	46.391	0.887
			Jul–Aug	-0.069	0.208	25.676	0.969
IJmondstroompaal	4.519	52.465	Jan–Feb	-0.091	0.308	50.503	0.865
			Jul–Aug	-0.052	0.168	30.316	0.954
K13a	3.219	53.218	Jan–Feb	-0.028	0.266	53.859	0.846
			Jul–Aug	0.022	0.135	30.847	0.956
K141	3.626	53.269	Jan–Feb	-0.03	0.283	56.636	0.828
			Jul–Aug	0.018	0.169	38.022	0.931
L91	4.87	53.566	Jan–Feb	-0.04	0.346	56.459	0.828
			Jul–Aug	-0.001	0.233	41.751	0.912
Oosterschelde11	3.48	51.64	Jan–Feb	-0.186	0.408	38.583	0.932
			Jul–Aug	-0.178	0.338	32.714	0.954
Q11	4.149	52.93	Jan–Feb	-0.04	0.292	58.62	0.812
			Jul–Aug	0.011	0.136	32.279	0.95
TerschellingNoordzee	5.333	53.443	Jan–Feb	-0.061	0.375	49.723	0.868
			Jul–Aug	-0.034	0.173	24.642	0.969
Wierumergronden	5.959	53.517	Jan–Feb	-0.078	0.38	47.486	0.88
			Jul–Aug	-0.054	0.199	26.483	0.965

Table 2.1: Model performance compared to tide gauges. Results computed over time windows of 2 months for year 2016. Scatter plots for model-TG elevations (all locations) are included in Appendix A.

(a) January to February 2016

(b) July to August 2016

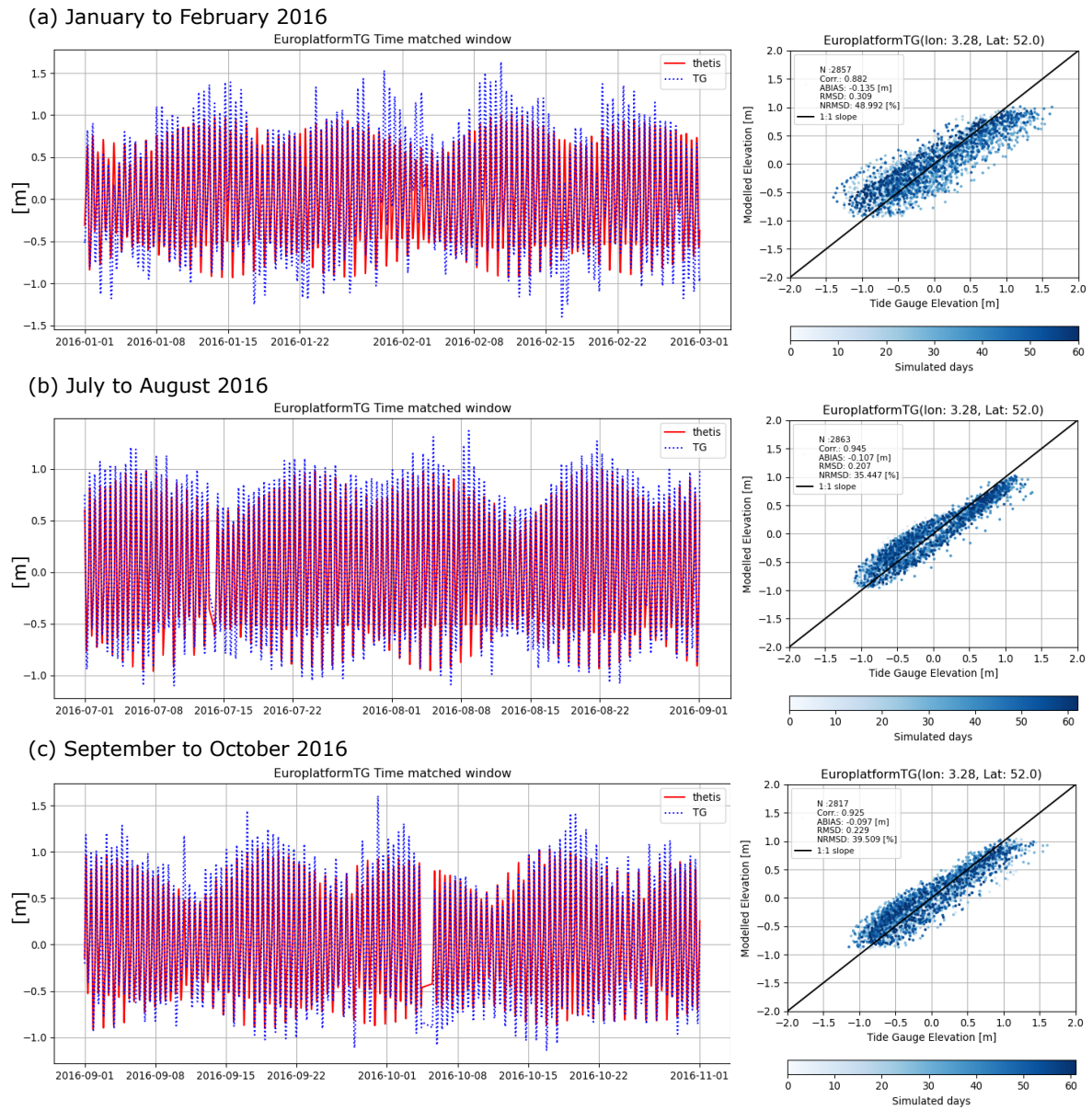

(c) September to October 2016

Figure 2.3: Model performance briefing at Europlatform TG. Analyzed time windows in year 2016: (a) January to February, (b) July to August, (c) September to October.
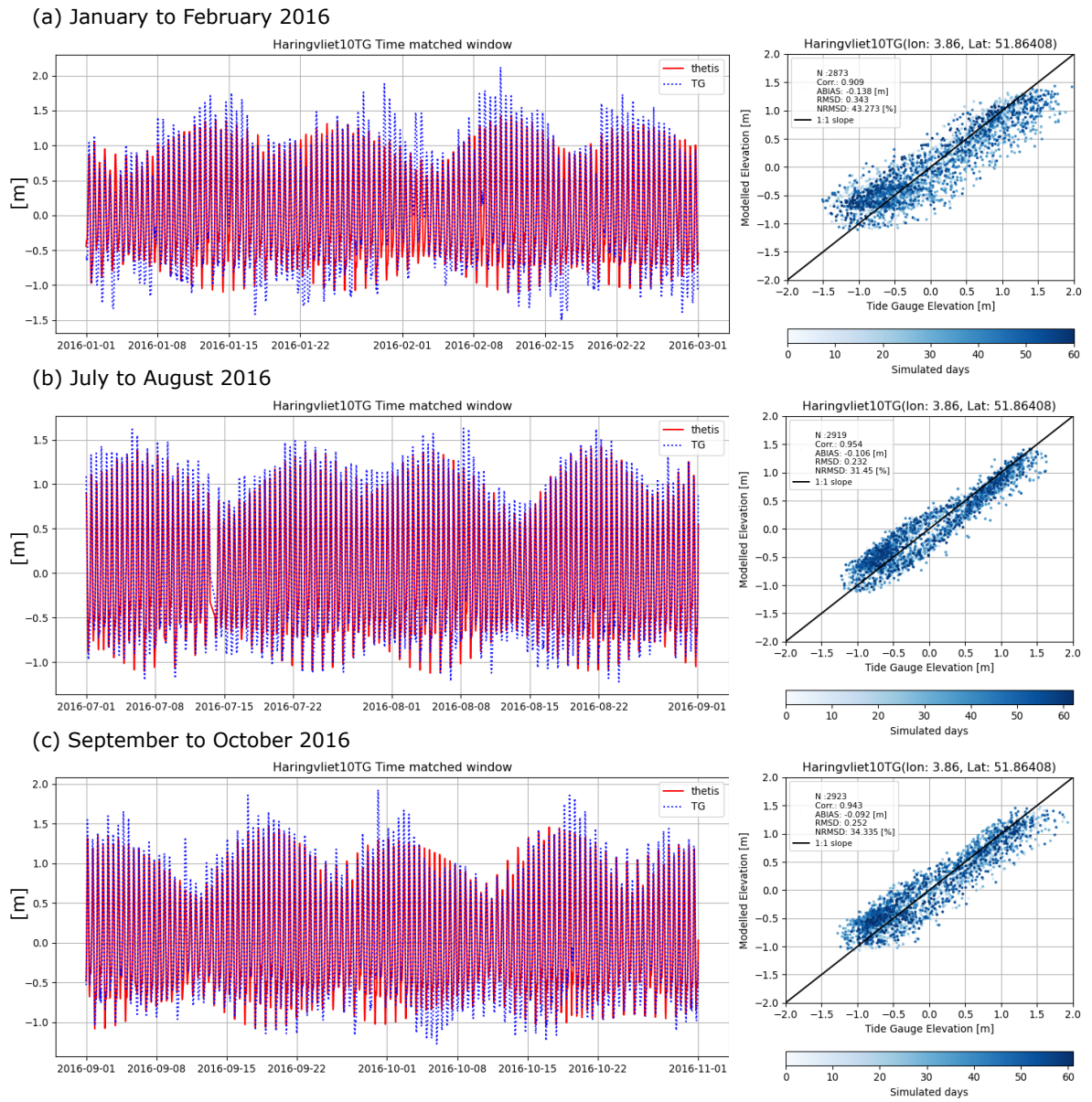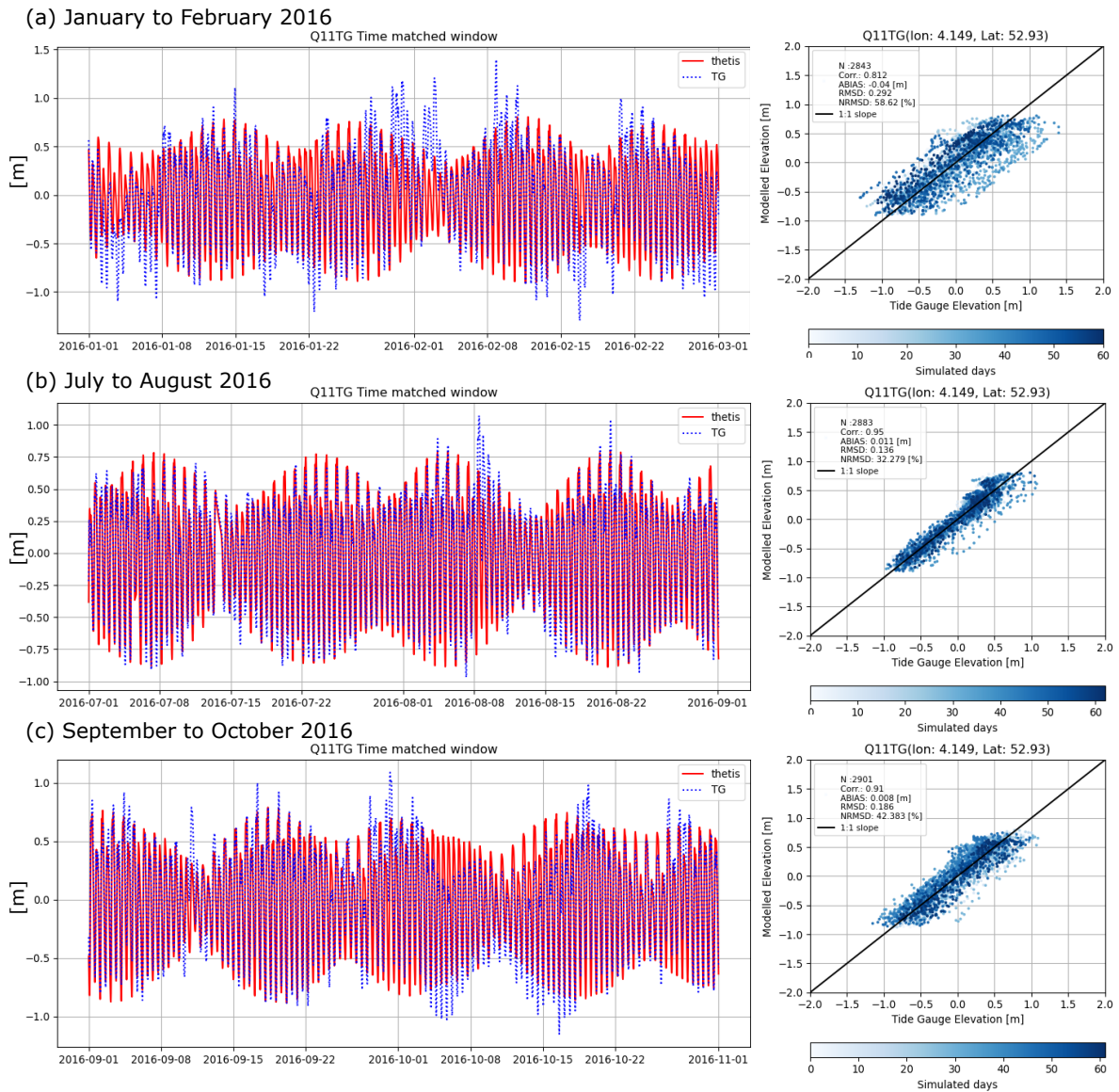
(a) January to February 2016

(b) July to August 2016

(c) September to October 2016

Figure 2.4: Model performance briefing at Haringvliet10 TG. Analyzed time windows in year 2016: (a) January to February, (b) July to August, (c) September to October.

Figure 2.5: Model performance briefing at Q11 TG. Analyzed time windows in year 2016: (a) January to February, (b) July to August, (c) September to October.

3

North Sea Tidal Database (NSTD)

Most studies analyzing tidal characteristics of the Dutch coast have typically focused on the role of this forcing in the context of deltas dynamics, tides-storm interactions and its effect on sediment transport, since it represents a key element for the maintenance of shipping routes and the stability of coastal structures [e.g. 20, 21, 24]. In recent years, and in the context of climate change effects, more efforts have been put into analyzing potential changes of the tidal regime in bays and inlets [e.g. 12, 17]. The lack of studies dedicated to the characterization of the Dutch stream tidal resource probably comes from its well know "low amplitudes". While high tidal ranges are typically desired for harnessing tidal power with barrages [e.g. 5, 8], areas without such evident potential for energy extraction can still present interesting velocities conditions due to the interaction of the tidal wave with the local topography.

In the present section we develop a complete analysis of the tidal stream potential along the Dutch coast based on a 1 year tides dataset. Special attention is paid to the flow conditions in the Westerchelde inlet in Zeeland, and in the surroundings of the West Frisian islands where the development of higher current intensities are observed.

3.1. Overview of current intensities

As seen in Fig. 3.1 mean and maximum current intensities due to astronomical tides do not have significant monthly variability, which is expected in a short term (< 1 year) analysis. Even though some variability in tidal ranges would be detected in long term analyses, for example when the nodal tide (18.6 years cycle) is considered [9], its effect is thought to be insignificant in developed intensities compared to the influence of strong atmospheric events like storm surges. One month averaged current intensities of ~ 0.4 to 0.6 m·s^{-1} are found in long open beaches and in general at distances from the coast > 20 km. Sightly higher mean values are observed in the Westerchelde inlet. In Fig. 3.1b is possible to see that particularly high intensities are developed between the western Frisian islands, namely Texel, Vlieland and Terschelling.

Two different approaches were used to characterize the tidal stream. First, to have an idea of the spatial variability we defined 5 transects representative of the areas of interest mentioned above, and computed the intensities probability distribution function (PDF) at every point defined for each transect (table 3.1). Then, as an attempt to characterize tidal stream resource availability per "zone", we computed the intensities PDF within 5 specific areas -around the same locations as the transects- integrating the time series from each mesh node contained within the analyzed area with depth >10 m. All computations are done over 2 months simulations.

The PDFs at the Westschelde transect show most frequent intensities of 0.8 and 0.7 m·s^{-1} with a relative occurrence of ~15% of the time. Intensities > 0.9 m·s^{-1} are also developed, particularly for Westschelde-02 we found a cumulative occurrence of ~18% for intensities >1.0 m·s^{-1} (Fig. 3.2a). Although along the defined transect we predict, in average, a cumulative occurrence of intensities ≥0.8 m·s^{-1} close to 30%, we note that this is a local behavior. When analyzing the complete area the overall occurrences peak drops to 0.6 m·s^{-1} while the cumulative occurrences distribution shows that 50% of the time the current intensities are smaller than 0.5 m·s^{-1} (Fig. 3.3a).

Most promising results are found along the Den Helder transect, where the PDFs of the nodes placed between Texel and Den Helder (01,02,03) show a less pronounced peak of occurrences (~9%) for intensities

Location Name	Nodes	East [m]	North [m]	Depth [m]
Westerschelde	01	541443.54	5696811.99	21.4
	02	538114.46	5696674.65	24.5
	03	535709.64	5697117.84	26.5
	04	533061.45	5696953.62	18.6
Den Helder	01	618822.41	5871437.61	24.7
	02	615943.70	5870597.35	31.4
	03	614556.99	5869209.36	28.7
	04	612633.56	5867358.20	20.1
De Cocksdorp	01	625680.47	5893628.62	7.0
	02	624891.01	5894697.68	8.2
	03	623607.03	5895705.62	7.8
	04	620899.89	5895720.27	7.0
Oost Vlieland	01	645031.81	5908906.75	18.6
	02	642763.88	5909848.44	12.5
	03	639312.29	5910361.10	14.5
	04	637054.58	5912018.97	14.6
Hollum	01	675982.48	5921559.41	13.7
	02	673476.21	5923702.28	19.5
	03	671687.81	5925428.00	7.0
	04	669657.02	5928193.20	7.0

Table 3.1: Transects used for intensities PDF construction. See locations in Appendix B.

of 1.6 m·s^{-1}, and where over 45% of the time estimated current intensities are ≥1.0 m·s^{-1} (Fig. 3.2b). For the complete area, the cumulative occurrences curve shows that 50% of the time intensities are ≥0.6 m·s^{-1} and 30% of the time ≥0.9 m·s^{-1}. In this case the lower intensities values (0.4 m·s^{-1}) at the peak of occurrences in the PDF (10%) are due to the contribution of the mesh nodes located offshore and away the passage between mainland and Texel, but notice that the occurrences differences between the peak and the intensities range 0.6 to 1.1 m·s^{-1} are only about 2% (Fig. 3.3b).

Although current intensities ≥1.1 m·s^{-1} are predicted at De Cocksdorp transect, the depths of the analyzed locations are < 10 m and even reach the minimum depth of 7 m imposed for numerical reasons (Fig. 3.2c). Results for the full area, considering depths ≥ 10 m show that almost all of the selected mesh nodes are placed offshore, where about 40% of the time current intensities are ≤0.3 m·s^{-1} and with maximum values of ~0.9 m·s^{-1} (Fig. 3.3c). The Hollum area present similar low intensities characteristics (Fig. 3.2e and 3.3e).

After the Den Helder area, the second location with higher simulated current intensities is Oost Vlieland, although larger variability in the position of the occurrences peak is observed between nodes. Intensities ≥1.2 m·s^{-1} are predicted at nodes 01 and 02, which are placed between Vlieland and Terchellig. Particularly for node Oost Vlieland-02 we estimate intensities ≥1.1 m·s^{-1} over 45% of the time (Fig. 3.2d). These high current locations are though to be local and probably nodes 03 and 04 are more representative of the full area conditions where we estimate that in average ~40% of the time currents are ≥0.6 m·s^{-1} with maximum intensities of ~1.5 m·s^{-1} (Fig. 3.3d).
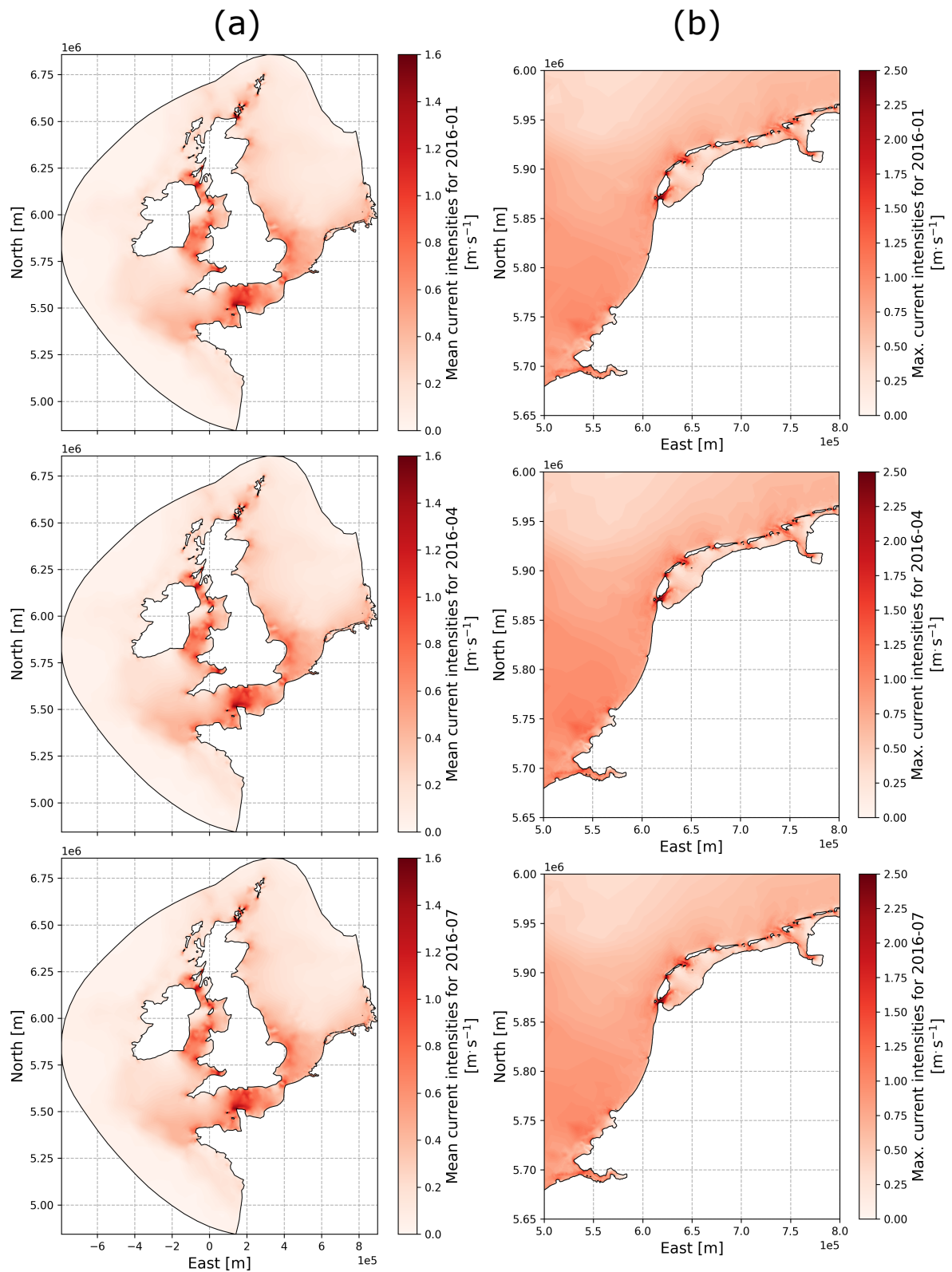
Figure 3.1: (a) Mean current intensities from January, April and July 2016 for the complete modelled domain. (b) Detail of the maximum current intensities along the Dutch coast. Mean and maximum current intensities are computed from the time series of each mesh node.
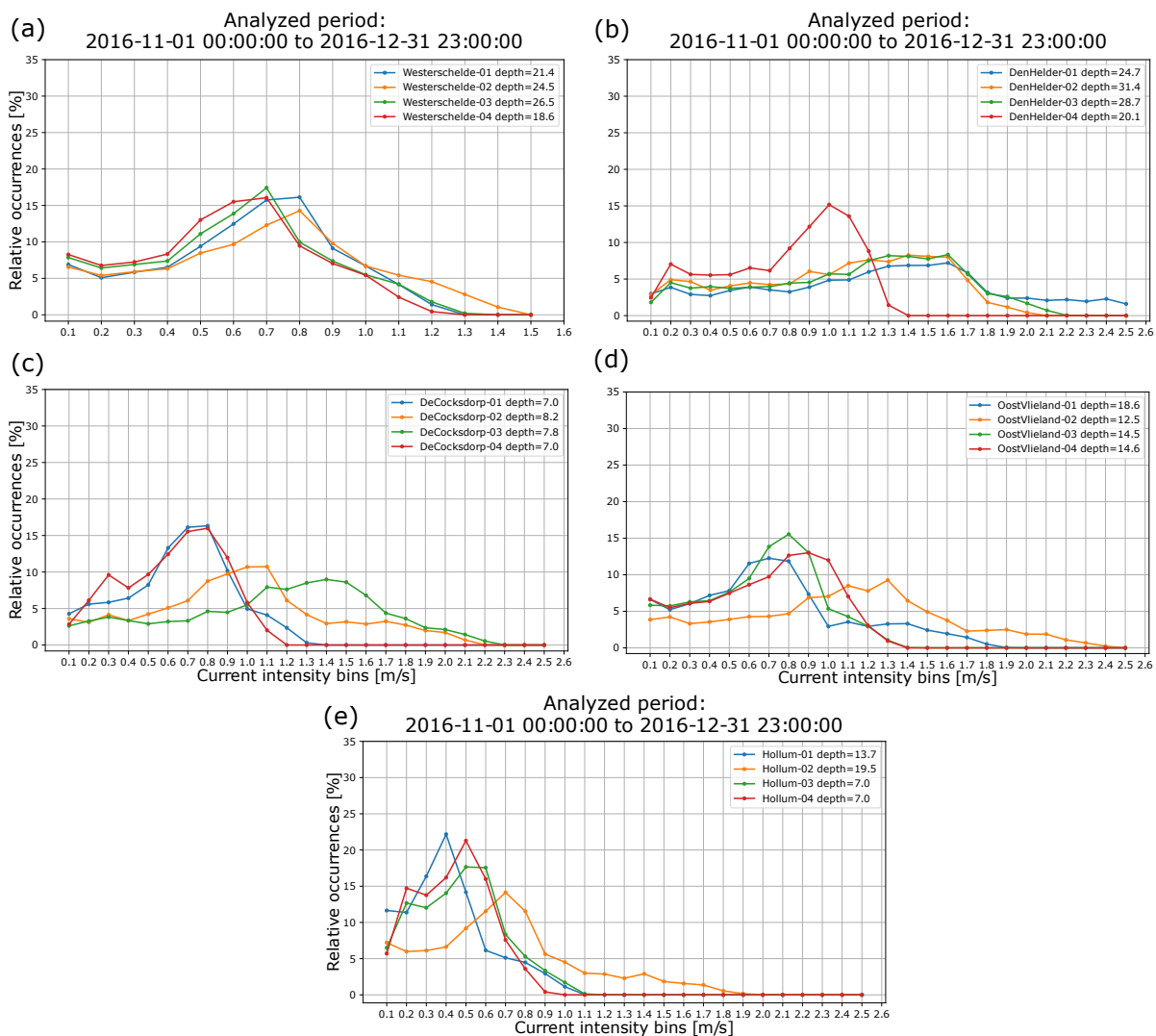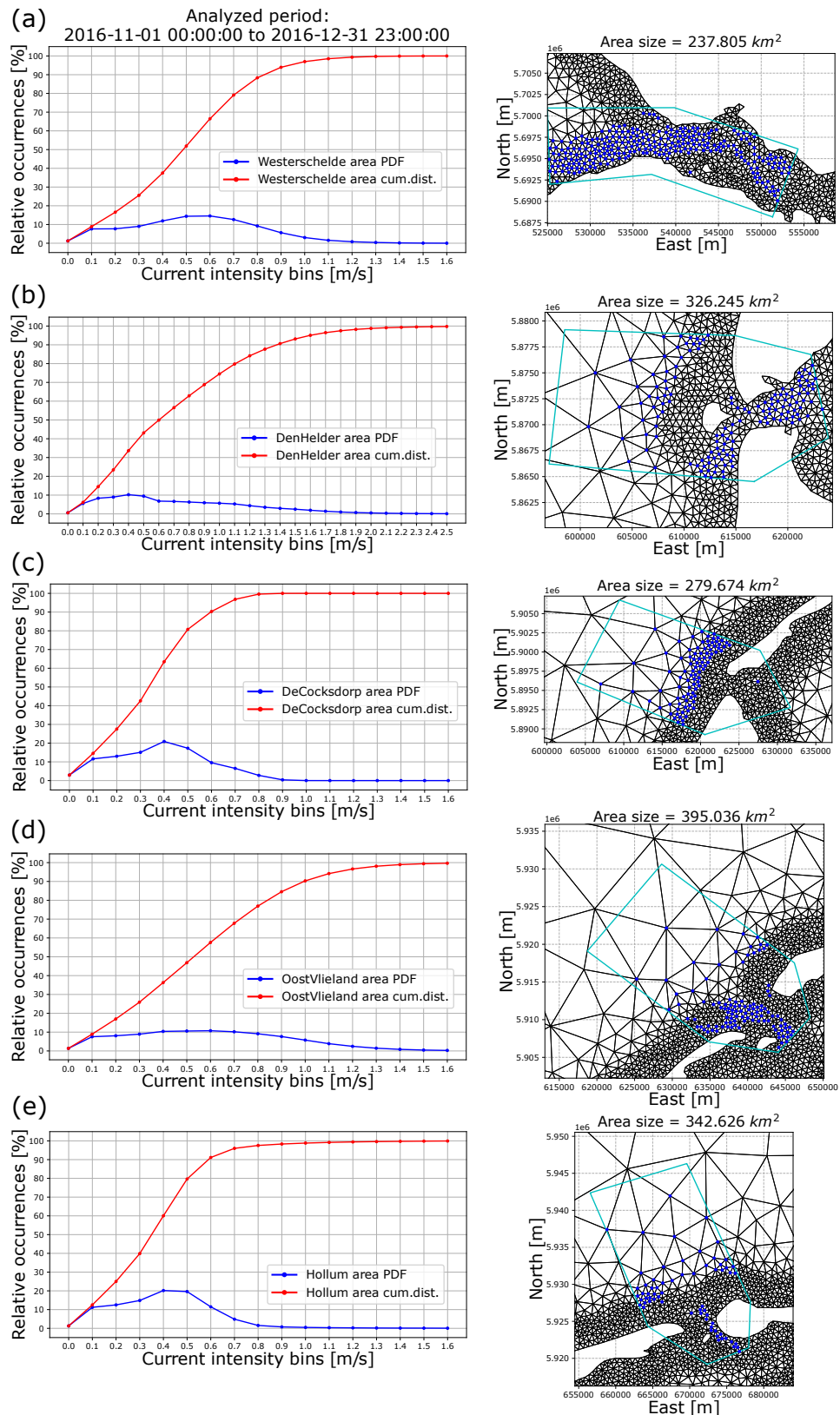
Figure 3.2: Intensities PDF computed along transects at (a) Westschelde, (b) Den Helder, (c) De Cocksdorp, (d) Oost Vlieland and (e) Hollum. Relative occurrences normalized by the total amount of analyzed data at each transect node. Intensities bin width is 0.1 m·s^{-1}. Specified nodes' depth is in meters with respect to the local mean sea level.

Figure 3.3: Intensities PDF computed at different areas: (a) Westschelde, (b) Den Helder, (c) De Cocksdorp, (d) Oost Vlieland and (e) Hollum. Mesh nodes in blue have an estimated depth > 10 m with respect to MSL. Relative occurrences normalized by the total amount of analyzed data with the contribution of all nodes in blue. Intensities bin width is 0.1 m·s^{-1}. The area size corresponds to the one defined by the polygon in cyan. Offshore extension of polygons for (b) to (e) is ~20 km.

3.2. **Tidal power density estimation**

The study of the current intensities' characteristics of the 5 selected areas helped to provide further details on potential sites adequate for deployment of tidal energy converters (TEC). The analyzed transects show local "hot spots" as Den Helder and Oost Vlieland where current intensities >1.0 m·s^{-1} can be found. Other locations like De Cocksdorp present interesting current conditions, but depths in the area might represent a problem for TEC operation. The estimation of the currents PDF per area also showed that particularly Den Helder and Oost Vlieland present intensities ≥0.6 m·s^{-1} over 40% of the time when all mesh nodes with depths >10 m are included in the analysis (actually over 50% of the time at Den Helder).

With a similar approach taken in section 3.1, here we present an overview of the tidal power density. First with a general look at mean and maximum W·m^{-2} along the Dutch coast, and then with more detailed view on those identified locations with higher current intensities.

The tidal power density in W·m^{-2} is computed as follows:

$$\left(\frac{P}{A}\right)_{water} = \frac{1}{2}\rho U^3 \tag{3.1}$$

where A is the cross-section area (in m^2) of flow intercepted by a TEC device, ρ is the water density in kg·m^{-3}, here taken as 1025 kg·m^{-3}, and U is the current intensity in m·s^{-1}.
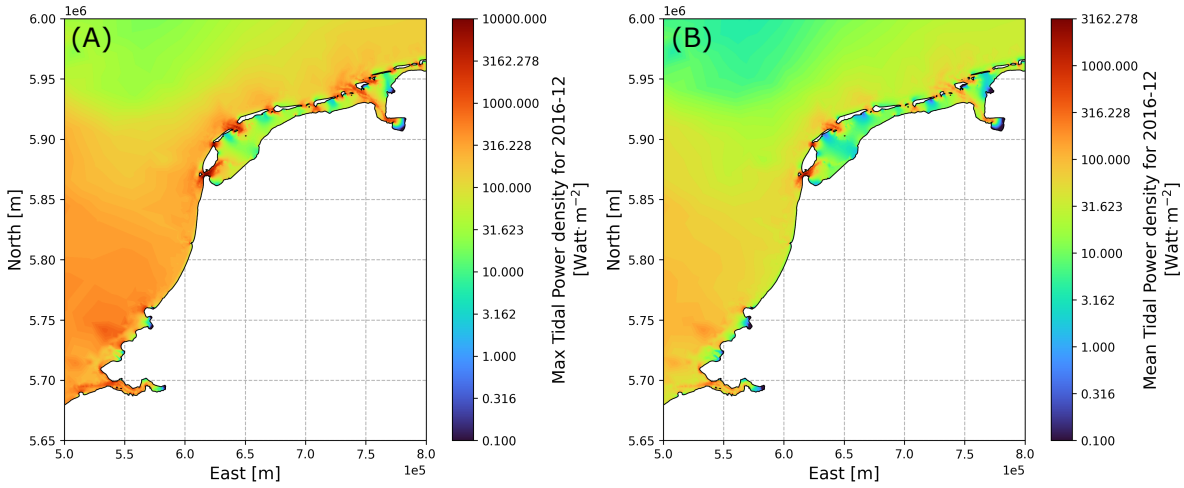

Figure 3.4: (a) Maximum and (b) mean tidal power density along the Dutch coast computed for December 2016.

In Fig. 3.4 we present the maximum and mean tidal power density estimated for December 2016. As shown in section 3.1, current intensities estimated from astronomical tides only, do not vary significantly along the year. Thus, the maximum and mean power density computed for December 2016 are considered representative of the most frequent conditions. From the general results in Fig. 3.4 is already noticed that even though there are maximum power density values of about 1 kW·m^{-2} within the Westschelde area, the mean shows considerable lower values of ~0.3 kW·m^{-2} in the most energetic areas (see Fig. 3.5a). Similar conditions are found at Oost vlieland and Hollum (Fig. 3.5d,e), although in these latter locations it was already expected given the low current intensities developed and most frequent speeds concentrated between 0.4 and 0.5 m·s^{-1} (Fig. 3.3e).

As expected, Den Helder presents the highest power density from the analyzed locations, with areas reaching values > 10 kW·m^{-2} (Fig. 3.5b). Additionally, it also presents the largest mean tidal power density (up to ~ 3 kW·m^{-2}), which is not only related to the development of higher current intensities, but also due to the more even intensities' distribution (or absence of a dominant occurrences peak; Fig. 3.2b and 3.3b). De Cocksdorp present similar high mean power density conditions, but as mentioned in section 3.1 shallow depths in this location may represent a problem for TEC operation.

Using the complete tides' database generated, we estimated the mean current intensities and corresponding mean power density for the complete dutch coast (Fig. 3.6). Additionally, the tidal power density distributions at the same transects described in table 3.1 are presented in Fig. 3.7. In this case, the transect at Hollum is not included since this area does not present interesting stream conditions.
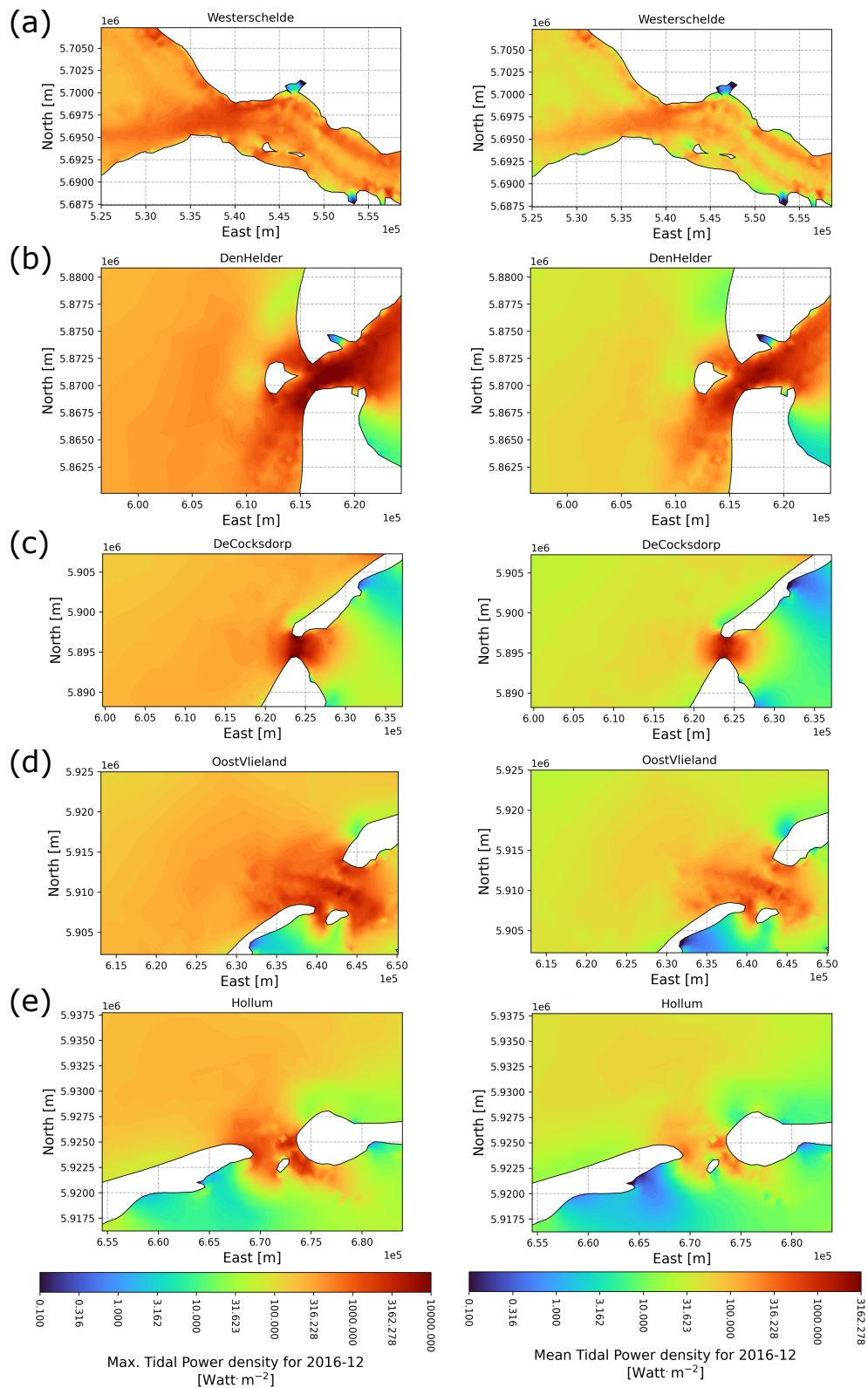
Figure 3.5: Maximum and mean tidal power density at (a) Westschelde, (b) Den Helder, (c) De Cocksdorp, (d) Oost Vlieland and (e) Hollum. Results from December 2016 simulation.

Notice that the mean intensities computed with 1 month time series (Fig. 3.4b) are practically equal to the yearly average in Fig. 3.6b. Basically, with 1 month simulation we captured the complete range of

intensities developed within the tidal cycle. In this sense, it is possible to consider the mean tidal power density computed for December 2016 (at specific locations) in Fig. 3.5b representative of the complete year. At the same time, the PDFs of intensities estimated per area in Fig. 3.3 are also representative of the complete year.
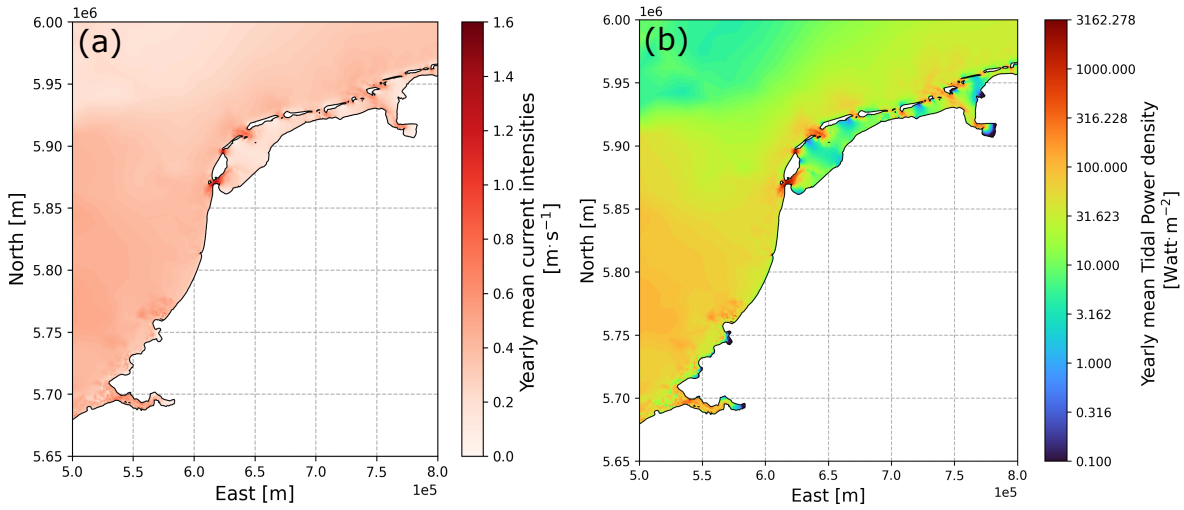
Figure 3.6: Yearly mean of (a) current intensities and (b) tidal stream power density. Results computed from full 2016 simulation.
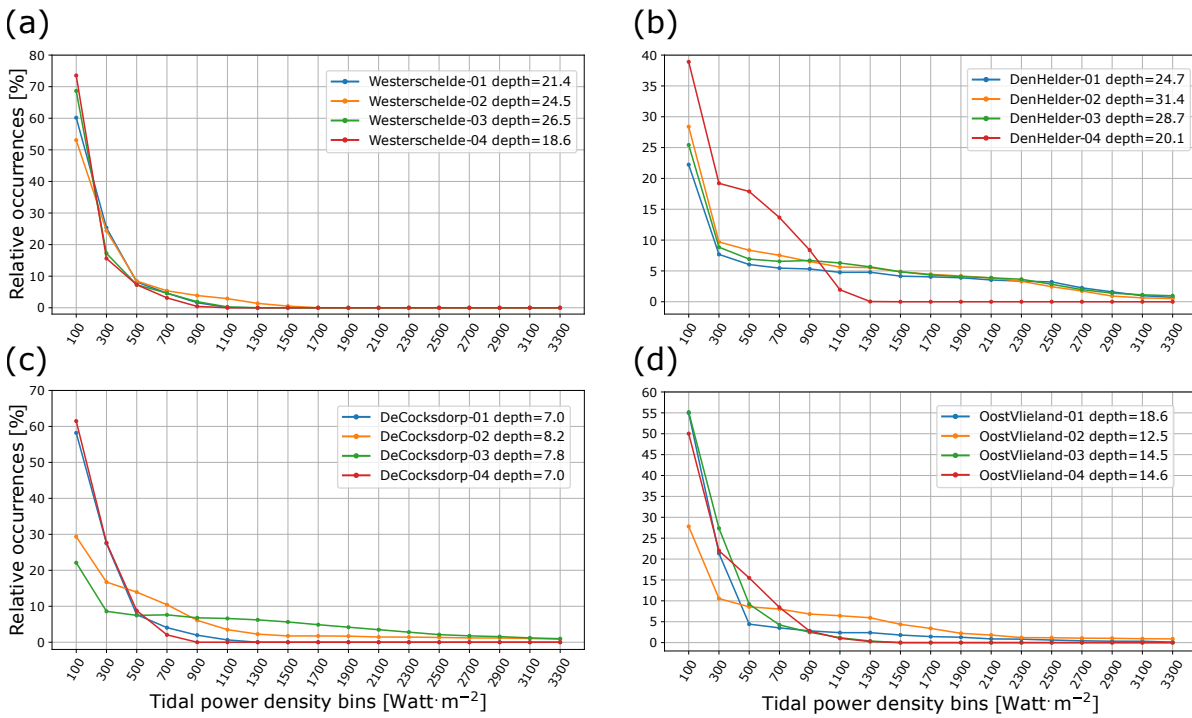
Figure 3.7: Tidal stream power density distributions at (a) Westschelde, (b) Den Helder, (c) De Cocksdorp and (d) Oost Vlieland transects. Results computed with full year 2016 simulation. Power density bins width is 200 W·m^{-2}. Transects' locations specified in table 3.1.

The power density distribution curves in Fig. 3.5 were computed using a bin width of 200 W·m^{-2}. In all defined transects the highest occurrences peak is located at 100 W·m^{-2} (meaning in the]0-200] W·m^{-2} range). This peak is specially high at the Westschelde transect reaching ∼75% in Westschelde-04. Along this transect the occurrences of higher power density drop significantly in all locations, with less than 30% at Westschelde-01 and 02 , and less than 20% at Westschelde-03 and 04 at 300 W·m^{-2}. It is estimated that only ∼26.5% of the time the stream power density is > 300 W·m^{-2} at Westschelde-04 and ∼47% of the time at Westschelde-02.

The latter location being the only one with occurrences of power density ≥900 W·m^{-2} (Fig. 3.7a).

Along the Den Helder transect, locations 01 to 03 present power density occurrences that 70% of the time are ≥ 300 W·m^{-2} and in average 45% of the time ≥ 900 W·m^{-2}. Given the current intensities' characteristics at Den Helder-04 (see Fig. 3.2), no power density occurrences ≥ 1300 W·m^{-2} are estimated, but it still presents 42% of the occurrences concentrated between 500 to 1100 W·m^{-2} (Fig. 3.7b).

At De Cocksdorp, locations 02 and 03 present the most interesting conditions of this transect, where we found power density values ≥ 500 W·m^{-2} 51% and 66% of the time respectively. De Cocksdorp-01 and 04 locations present the minimum depth threshold imposed in the model, which is partly why these results should be revisited in future studies (Fig 3.7c).

Finally, for Oost Vlieland at locations 01, 03 and 04 we found power density values ≥ 300 W·m^{-2} 45% of the time and more. Particularly, the highest values are found at Oost Vlieland-02 where 45% of the time the power density obtained is ≥ 700 W·m^{-2} and almost 40% ≥ 900 W·m^{-2} (Fig. 3.7d). These results confirm that Den Helder and Oost Vlieland are the areas with higher potential for energy extraction along the Dutch coast.

Analog to the current intensities PDF generated per area from Fig. 3.3, power density PDFs were generated considering the contribution of all mesh nodes with depth larger than 10 m within a specific zone. Nodes' selection was done using a more adjusted area, which was defined taking into account the higher mean values presented in Fig 3.5. In this case, the PDF curves were computed using the complete 1 year dataset with tidal power density bins of 100 W·m^{-2} and only for the areas considered to have the higher potential for energy extraction, Den Helder and Oost Vlieland (Fig. 3.8). Notice that the areas' selection has been done excluding land.
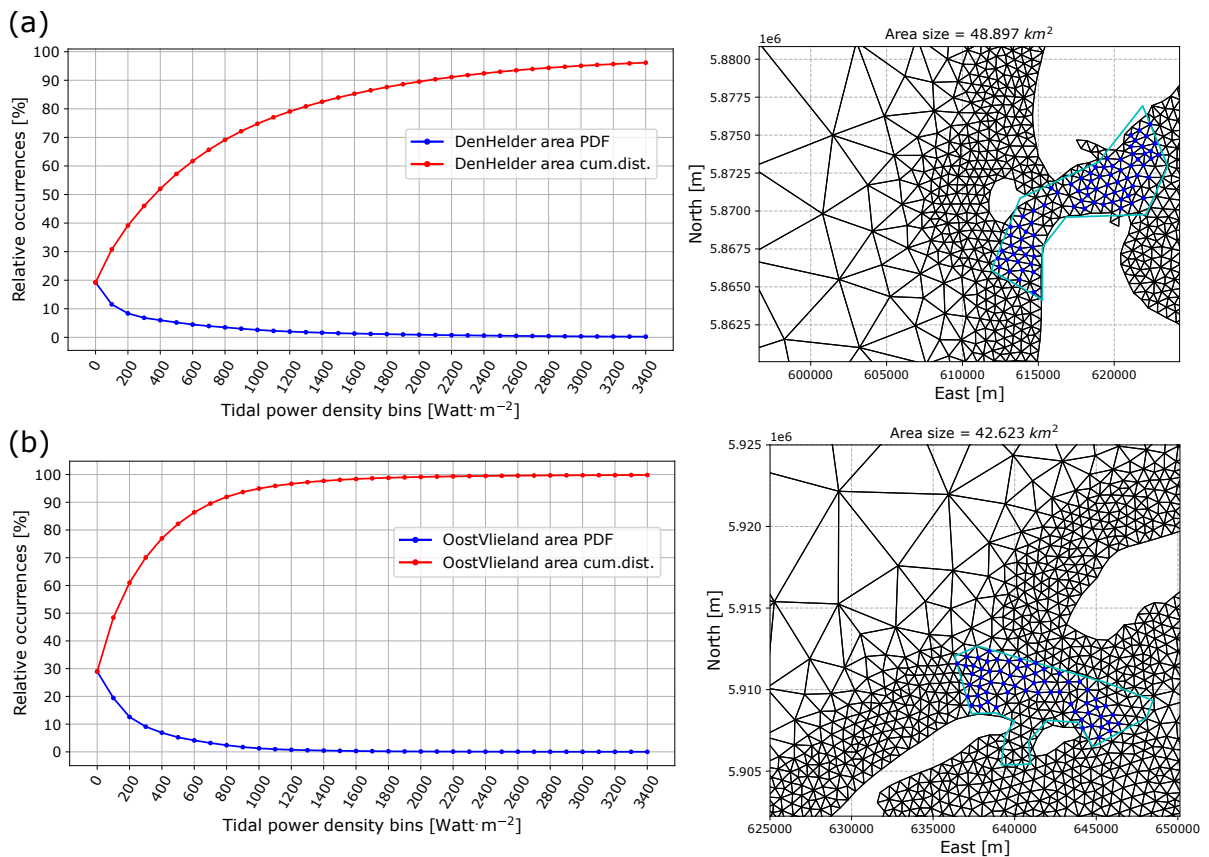

Figure 3.8: Tidal stream power density distributions at (a) Den Helder and (b) Oost Vlieland areas. Results computed with full year 2016 simulation. Power density bins width is 100 W·m^{-2}. The area size corresponds to the one defined by the polygon in cyan. In blue, mesh nodes with depth > 10 m.

When considering the contribution of all selected nodes in the Den Helder area, in average 55% of the time the power density is ≥ 300 W·m^{-2} and only ~ 27% of the time ≥ 900 W·m^{-2} (Fig. 3.8a), which suggest that probably the most "energetic" locations are placed in the neighborhood of the previously analyzed transect. The Oost Vlieland area PDF (Fig. 3.8b) presents power density levels ≥ 300 W·m^{-2} 30% of the time, 15% lower than in the locations along the transect previously analyzed and power density levels ≥ 900 W·m^{-2} less than

10% of the time, similar to locations 03 and 04 in the Oost Vlieland transect (Fig. 3.7d). With these results, it is expected that the higher power density levels of this area are found in the surroundings of location Oost Vlieland-02.

4

Conclusions

In the preset document we have developed the first tidal stream assessment for Dutch waters using a high resolution tide model specially adjusted for this purpose. The main objective of this study was to characterize and identify areas with potential for energy extraction along the coast of The Netherlands. To perform the tidal stream characterization, a 1 year database of currents and elevation was generated using the implemented model.

With an overview of monthly mean and maximum tidal current intensities, an initial selection of 5 zones was made to further analyze their stream characteristics. Westchelde, Den Helder, De Cocksdorp, Oost Vlieland and Hollum presented the higher mean current speed values. Characterization of these areas was done using the intensities probability distribution function (PDF), first at discrete locations along transects, and then integrating the intensities time series from a set of mesh nodes contained within an arbitrary area. The latter approach helped to provide a more general view of the intensities distribution within the zones of interest. The stronger current speeds were found at Den Helder, Oost vlieland and De Cocksdorp presenting locations that develop intensities higher than 1.5 m·s^{-1}. Although simulations show high intensities in De Cocksdorp, the shallow depths (< 10 m) of the analyzed area may represent a problem for installation and operation of tidal stream energy converters (TEC).

In general Den Helder presented the highest current intensities with also high occurrences in time. We found that at particular locations over 45% of the time the estimated intensities are ≥1.0 m·s^{-1}, and for the complete area, the cumulative occurrences curve shows that in average 50% of the time intensities are ≥0.6 m·s^{-1} and 30% of the time ≥0.9 m·s^{-1}. Oost Vlieland also presented interesting results at specific locations, with intensities ≥1.1 m·s^{-1} over 45% of the time, but these values are highly local. For the complete area we found that 40% of the time intensities are ≥0.6 m·s^{-1}.

With the current intensities characteristics well defined per area, a similar analysis was done using the 1 year dataset to compute the power density distributions. As expected, given their tidal currents' characteristics, Den Helder and Oost Vlieland presented the higher stream power density levels. At the Den Helder area it was found that in average 55% of the time the stream power density is ≥ 300 W·m^{-2} and about 27% of the time ≥ 900 W·m^{-2}. Higher power density levels were found along the transect defined in this area, with locations that 45% of the time present power density levels ≥ 900 W·m^{-2}. When considering the complete analysis area, Oost Vlieland's power density PDF showed power density values ≥ 300 W·m^{-2} 30% of the time and values ≥ 900 W·m^{-2} less than 10% of the time. It is thought that the highest power levels in Oost Vlieland are mostly located in the proximity of the transect defined to analyze particular locations, particularly close to Oost Vlieland-02 where it was estimated that 45% of the time the stream power density is ≥ 700 W·m^{-2} and about 40% of the time ≥ 900 W·m^{-2}.

It should be noted that even though PDFs computed per area helped to provide an idea of the mean current or power density conditions per zone, the results are highly affected by the actual limits of the selected area. This is why we finally adjusted the area selection at Den Helder and Oost Vlieland after having analyzed the mean current characteristics.

5

Recommendations

This work quantifies the potential of the Dutch Exclusive Economic Zone (EEZ) for tidal stream technologies. From hereafter the tidal stream resource will correspond to the tidal resource. From the obtained results, the authors' team provide some recommendations for future development. We anticipate that our recommendations, will be beneficial to further research, reduction of uncertainties, model improvements, and positive developments of Dutch based companies.

It has to be evident that resource quantification, and spatio-temporal resolution are the basis for technical and economic development of tidal projects. We have considered some simplification for the present study, mainly to ensure numerical stability and in terms of forcing included in the model used to investigate the whole of the Netherlands in a high resolution mesh.

In general the tidal resource of the Netherlands is classified as low density. Therefore, existing tidal turbines from more mature markets will not be useful, thus, the adaptation/development of low stream tidal turbines is a vital step is to make the use of the available resource feasible.

Future research recommendations:

1. Coupling tidal model with high-resolution wave, to improve interaction resolution.

2. Definition of minimum depth limit and consideration of dry-wet effects for further analysis in the Wadden Sea and Frisian islands.

3. Spatial optimisation of bottom friction level to improve representation of elevations and currents.

4. Use of specific flow velocities from Acoustic Doppler Current Profiler (ADCP) to reduce uncertainties for research and industry. Deployment of ADCP, gather results, decluster, filter noise, and publish results for research and industry.

5. Enhance collaboration with developers to re-structure their devices for the Netherlands, assess optimal power performance and minimise loading.

6. Research the impacts of tidal array configuration both in latitudal and longitudal distances, and investigate both staggered and non-staggered approaches.

7. Expand to the use of a 3D model that way elevation velocity profiles and sediment transport can be better resolved, in presence of tidal arrays.

8. Assess the noise from tidal arrays and its environmental impact.

9. Optimise tidal arrays configuration for optimal power production or minimisation of sediment transport.

Since only astronomical tides were considered, we have employed a depth-averaged hydrodynamic model, which is well suited for this type of forcing. With the coupling of a high resolution wave and current detection mode of seasonal changes in the time series of elevations, and flows can be improved significantly.

The definition of a shallower minimum depth limit and improving inclusion of wet and dry effects should be further analyzed for the implementation of a high resolution model of the Wadden Sea including wet and dry (flooding) in the simulations.

The spatially homogeneous bottom friction value used in the model was defined after a sensitivity analysis of the simulated water elevation time series compared to the in situ data from the selected tide gauges.

Although this approach helped to reduce tidal amplitude errors in most analyzed locations it can also introduce spurious results elsewhere. Given the cumulative effect of the bottom friction it is expected that a more detailed representation, considering spatial changes related to bottom sediment types will help to improve the accuracy of the simulated levels and velocities.

Finally, calibration and validation of the implemented model was done only against time series of elevations. Even though an overall reduced amplitudes' bias and high correlation values were obtained, this does not necessarily extrapolates to the simulated velocity components (u and v), specially in areas with intricate bathymetry features.

In order to further adjust the model, reduce uncertainty of the simulations and fully validate the results, which in the end will be translated into a more accurate tidal resource assessment, it is necessary to perform in situ measurements with ADCPs for at least 30 days in the summer and winter seasons. It is expected that with the proposed improvements an substantial increase in accuray can be achieved for the simulated levels and intensities within Dutch tidal resources.

Appendix

A. Model validation against tide gauges

In this section we present the model performance results comparing with the 13 tide gauges selected along the Dutch coast.
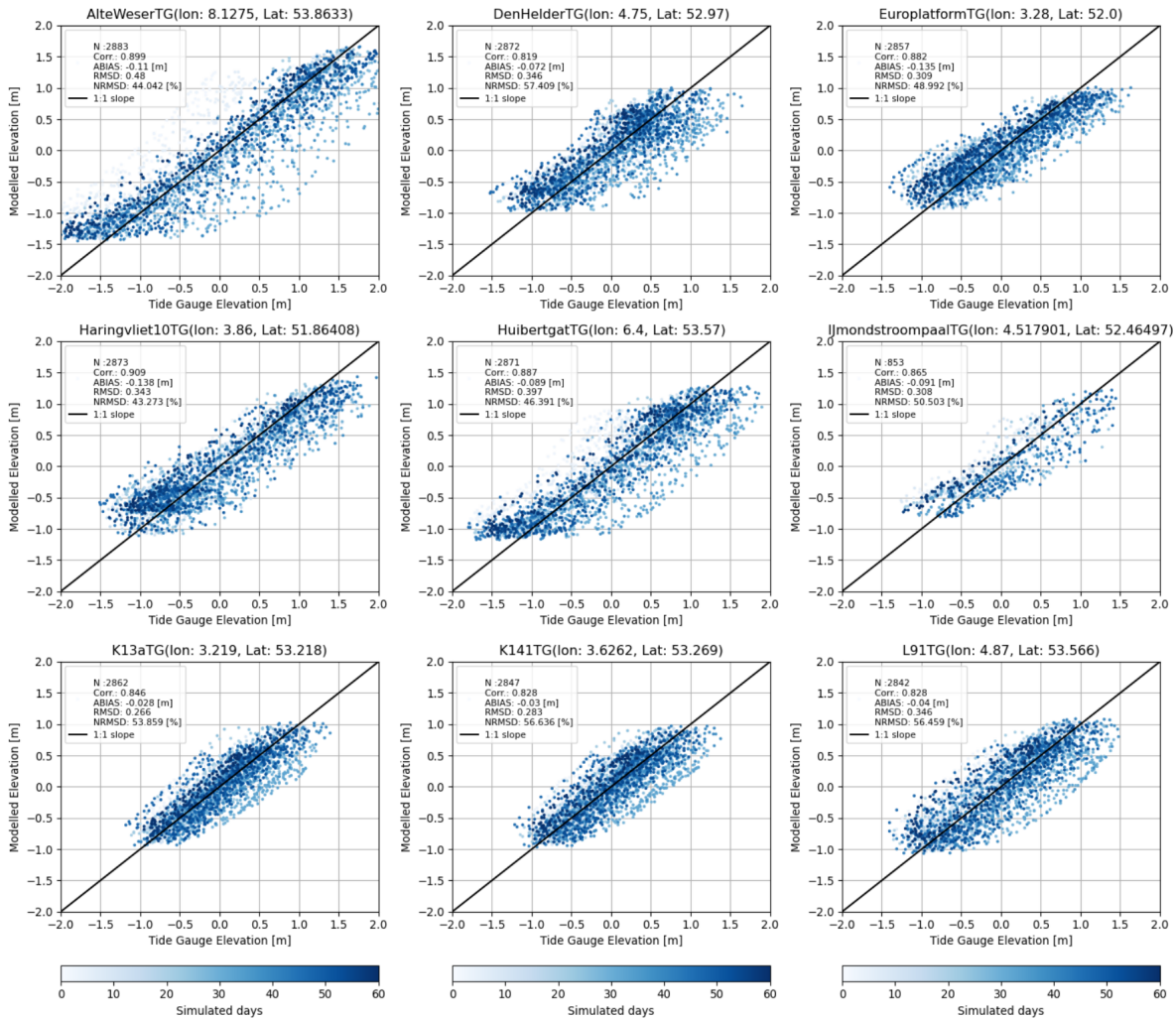

Figure A.1: Performance parameters for January-February 2016. Tide gauges locations: Alte Weser, Den Helder, Euro Platform, Haringvliet, Huibertgat, IJmond stroompaal, K13a, K141 and L91.
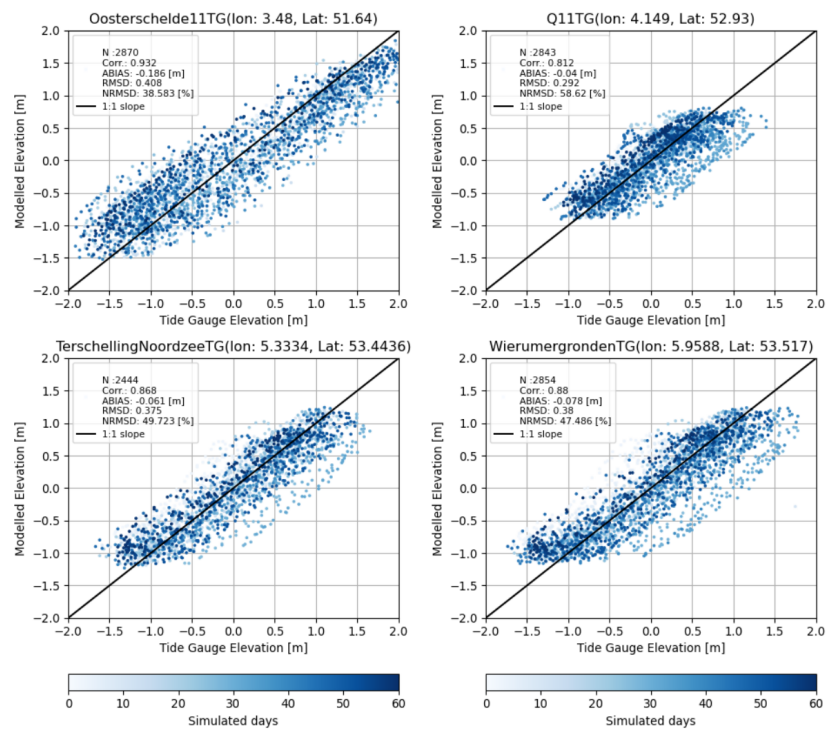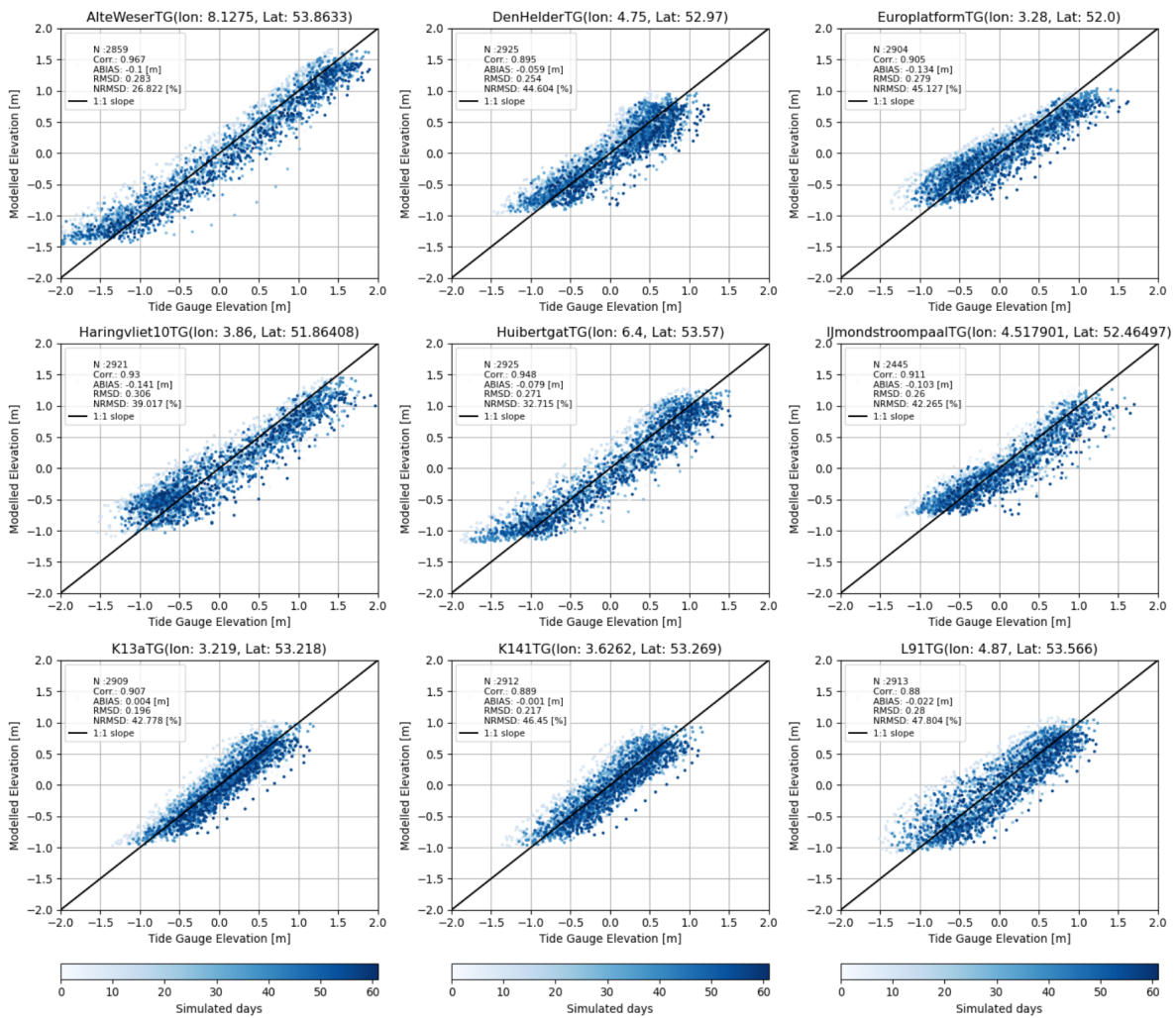
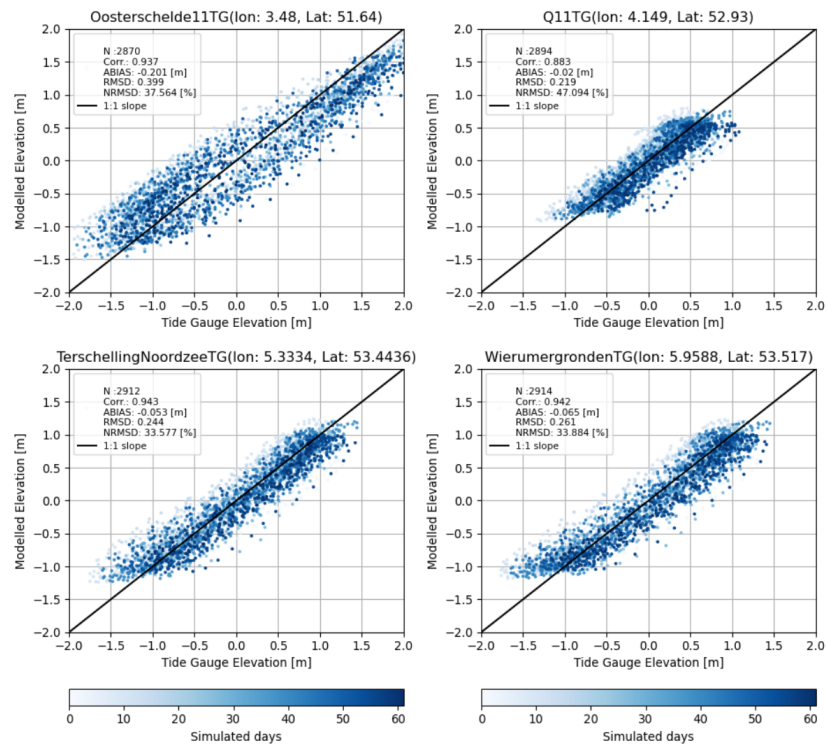Figure A.2: Performance parameters for January-February 2016. Tide gauges locations: Ooster Schelde, Q11, Terschelling Noordzee, Wierumergronden.
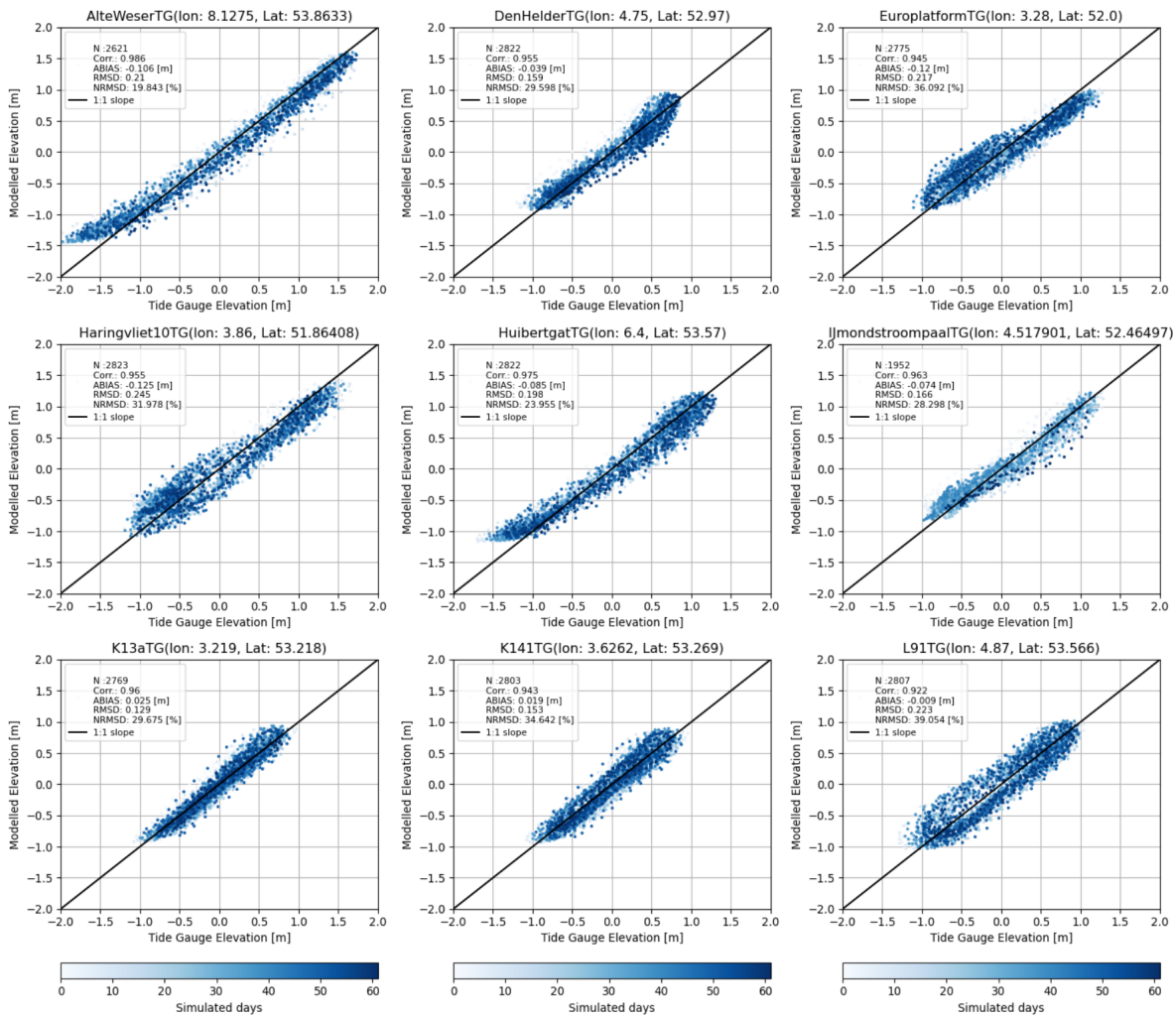
Figure A.3: Performance parameters for March-April 2016. Tide gauges locations: Alte Weser, Den Helder, Euro Platform, Haringvliet, Huibertgat, IJmond stroompaal, K13a, K141 and L91.
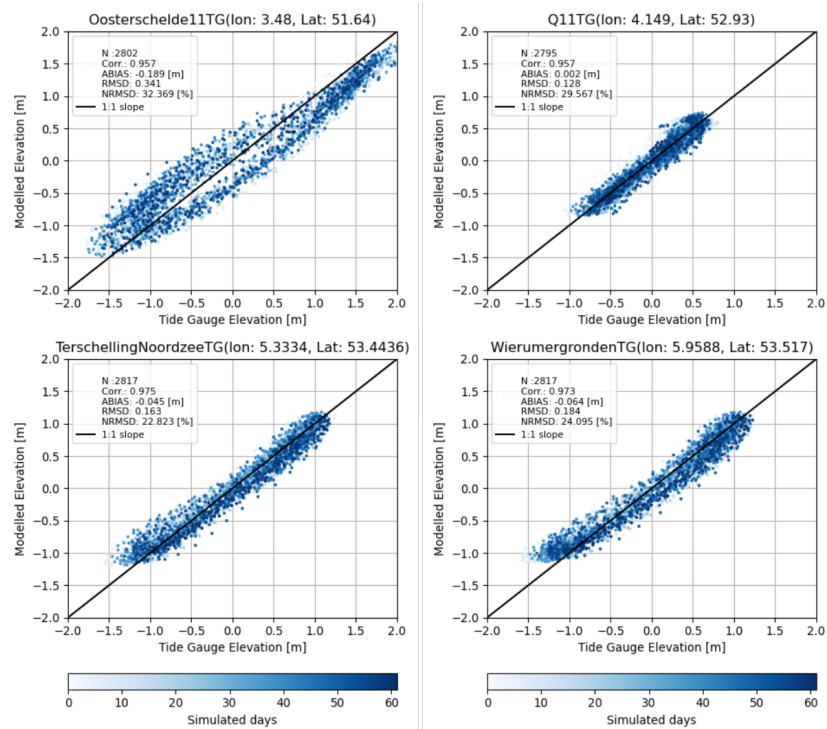
Figure A.4: Performance parameters for March-April 2016. Tide gauges locations: Ooster Schelde, Q11, Terschelling Noordzee, Wierumergronden.

Figure A.5: Performance parameters for May-June 2016. Tide gauges locations: Alte Weser, Den Helder, Euro Platform, Haringvliet, Huibertgat, IJmond stroompaal, K13a, K141 and L91.

Figure A.6: Performance parameters for May-June 2016. Tide gauges locations: Ooster Schelde, Q11, Terschelling Noordzee, Wierumergronden.
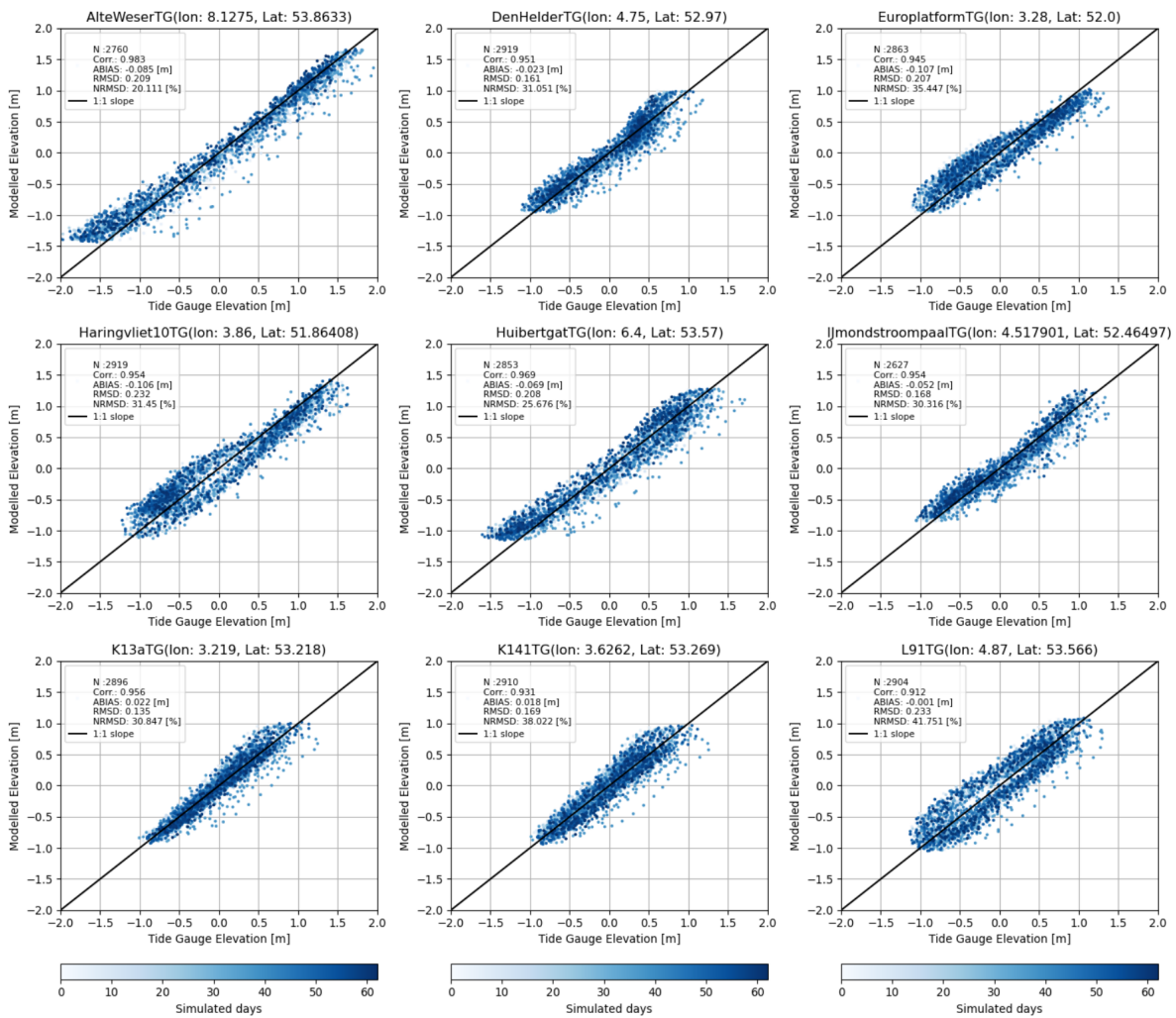
Figure A.7: Performance parameters for July-August 2016. Tide gauges locations: Alte Weser, Den Helder, Euro Platform, Haringvliet, Huibertgat, IJmond stroompaal, K13a, K141 and L91.
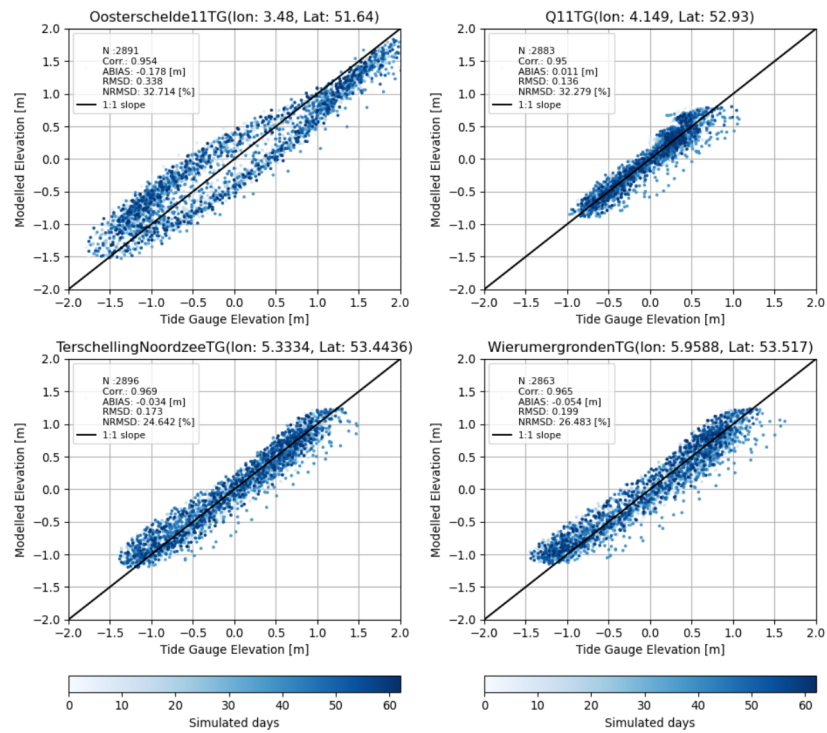
Figure A.8: Performance parameters for July-August 2016. Tide gauges locations: Ooster Schelde, Q11, Terschelling Noordzee, Wierumer-gronden.
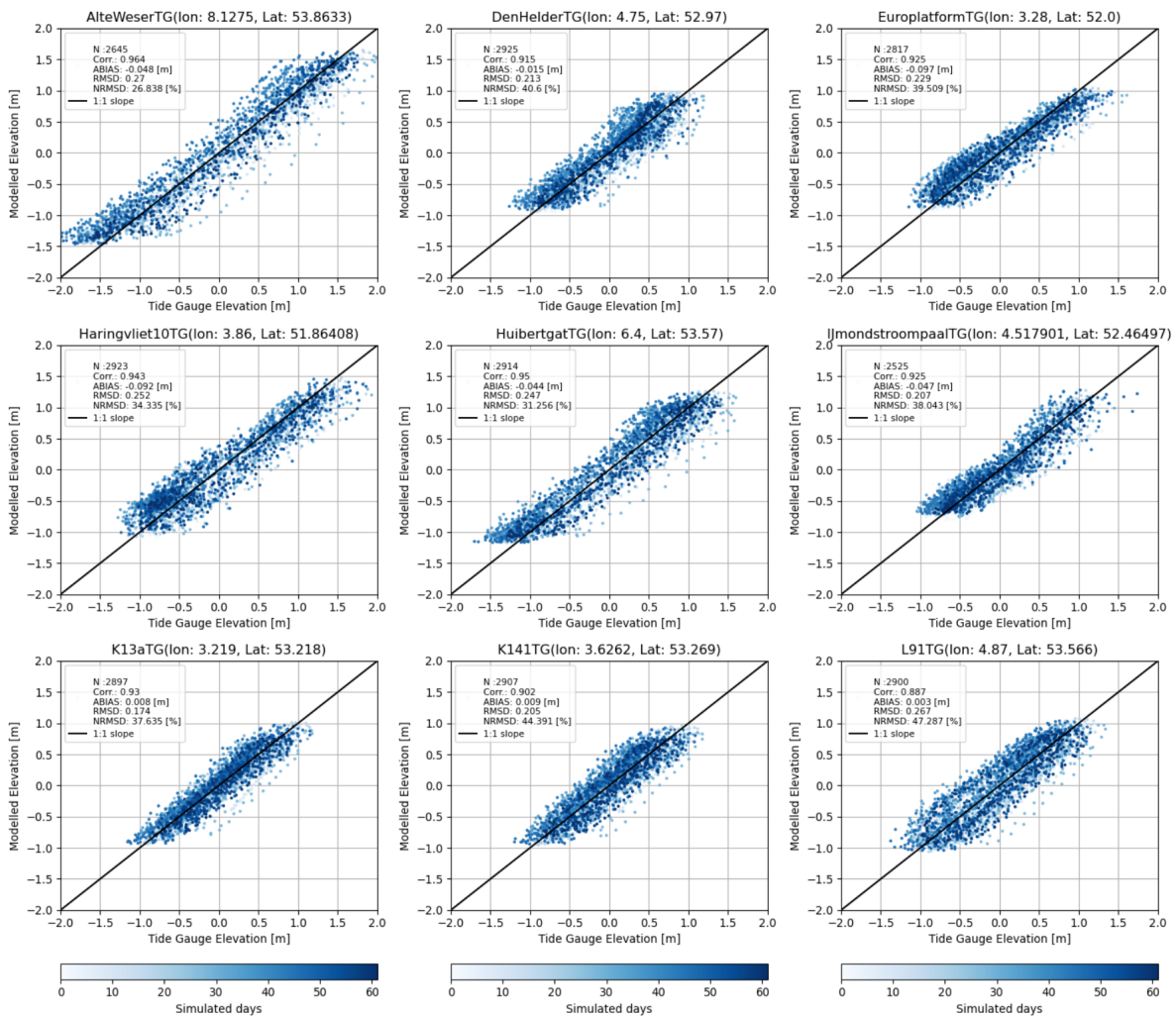
Figure A.9: Performance parameters for September-October 2016. Tide gauges locations: Alte Weser, Den Helder, Euro Platform, Haringvliet, Huibertgat, IJmond stroompaal, K13a, K141 and L91.
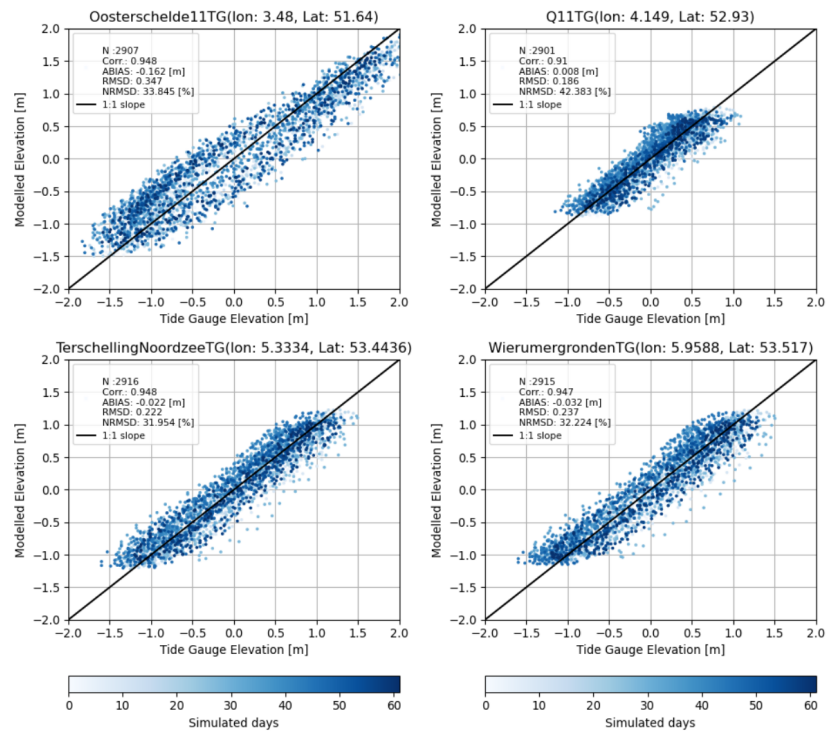
Figure A.10: Performance parameters for September-October 2016. Tide gauges locations: Ooster Schelde, Q11, Terschelling Noordzee, Wierumergronden.
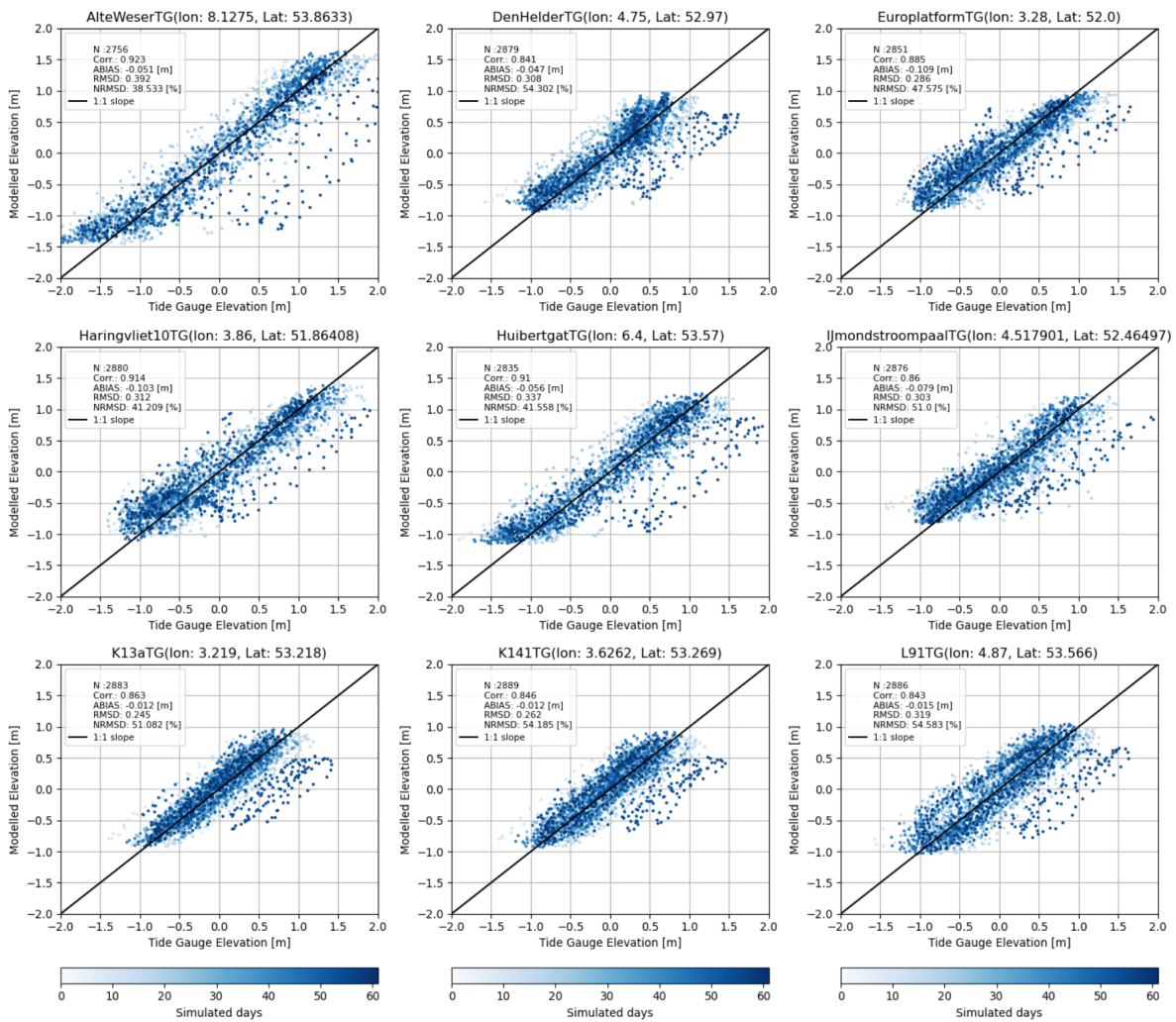
Figure A.11: Performance parameters for November-December 2016. Tide gauges locations: Alte Weser, Den Helder, Euro Platform, Haringvliet, Huibertgat, IJmond stroompaal, K13a, K141 and L91.
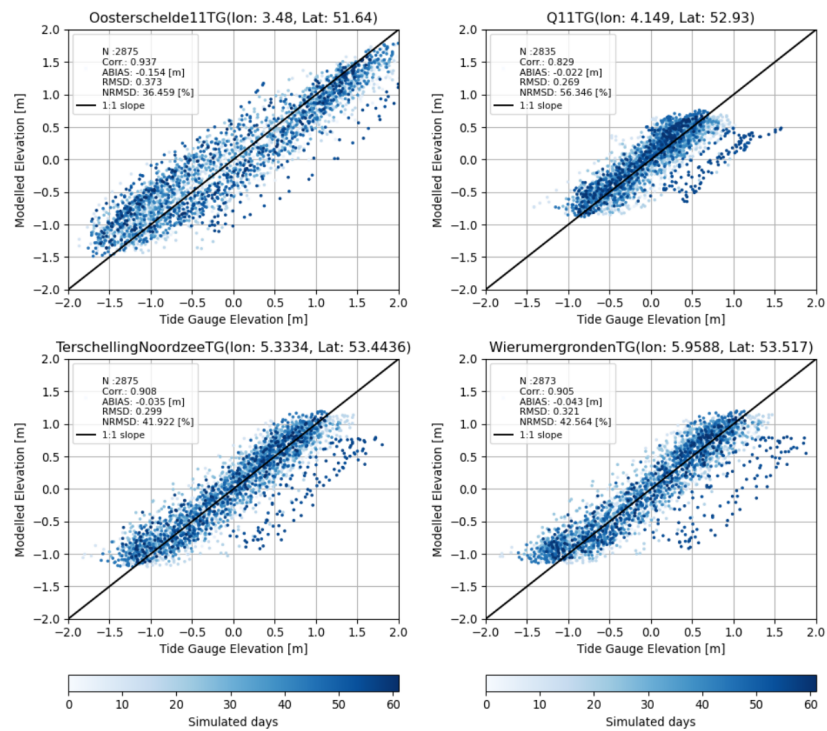
Figure A.12: Performance parameters for November-December 2016. Tide gauges locations: Ooster Schelde, Q11, Terschelling Noordzee, Wierumergronden.

B. Transects locations for current and power density characterization

The following figures show the location of the the transects defined in Chapter 3 for the analysis of current intensities and power density distribution.

Figure B.1: Selected locations at (a) Den Helder and (b) De Cocksdorp areas.
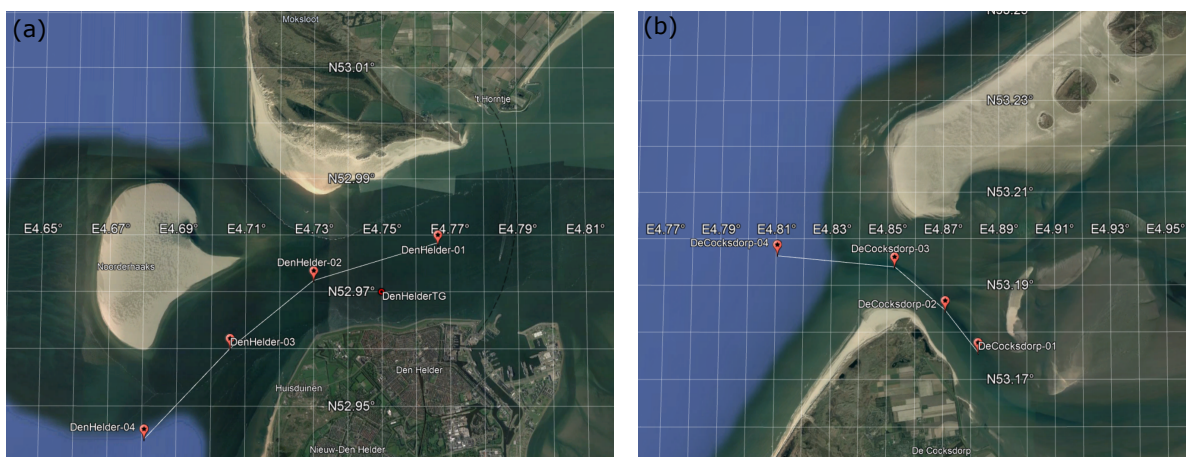

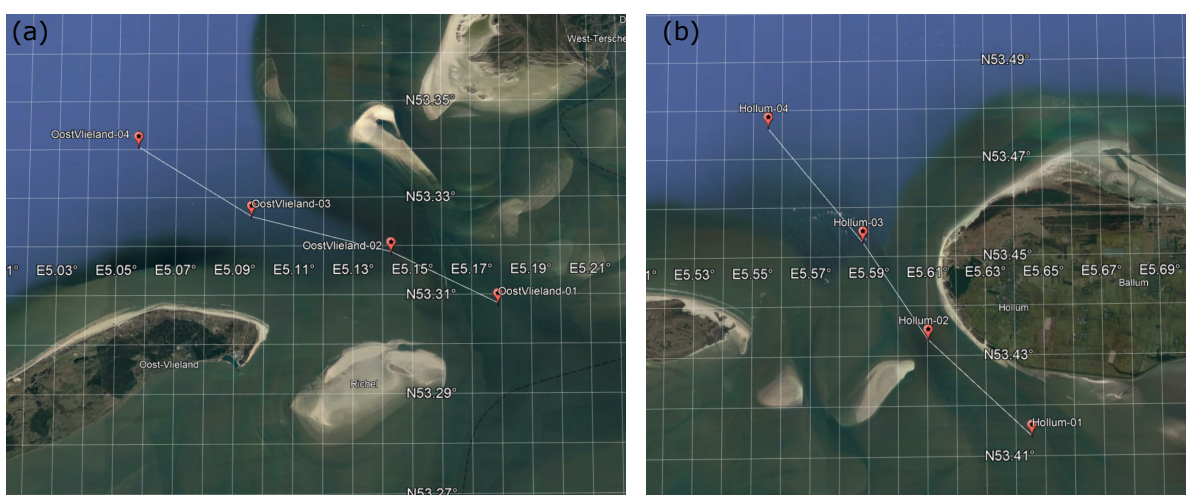Figure B.2: Selected locations at (a) Den Helder and (b) De Cocksdorp areas.

Figure B.3: Selected locations at (a) Oost Vlieland and (b) Hollum areas.

Bibliography

[1] Uri M. Ascher, Steven J. Ruuth, and Brian T. R. Wetton. Implicit-explicit methods for time-dependent partial differential equations. *SIAM Journal on Numerical Analysis*, 32(3):797–823, 1995. doi: 10.1137/0732037. URL https://doi.org/10.1137/0732037.

[2] Alexandros Avdis, Adam S Candy, Jon Hill, Stephan C Kramer, and Matthew D Piggott. Efficient unstructured mesh generation for marine renewable energy applications. *Renewable Energy*, 116:842–856, 2018.

[3] Satish Balay, William D. Gropp, Lois Curfman McInnes, and Barry F. Smith. Efficient management of parallelism in object oriented numerical software libraries. In E. Arge, A. M. Bruaset, and H. P. Langtangen, editors, *Modern Software Tools in Scientific Computing*, pages 163–202. Birkhäuser Press, 1997.

[4] Satish Balay, Shrirang Abhyankar, Mark F. Adams, Steven Benson, Jed Brown, Peter Brune, Kris Buschelman, Emil Constantinescu, Lisandro Dalcin, Alp Dener, Victor Eijkhout, William D. Gropp, Václav Hapla, Tobin Isaac, Pierre Jolivet, Dmitry Karpeev, Dinesh Kaushik, Matthew G. Knepley, Fande Kong, Scott Kruger, Dave A. May, Lois Curfman McInnes, Richard Tran Mills, Lawrence Mitchell, Todd Munson, Jose E. Roman, Karl Rupp, Patrick Sanan, Jason Sarich, Barry F. Smith, Stefano Zampini, Hong Zhang, Hong Zhang, and Junchao Zhang. PETSc/TAO users manual. Technical Report ANL-21/39 - Revision 3.17, Argonne National Laboratory, 2022.

[5] R Burrows, NC Yates, TS Hedges, M Li, JG Zhou, DY Chen, IA Walkington, J Wolf, J Holt, and R Proctor. Tidal energy potential in uk waters. In *Proceedings of the Institution of Civil Engineers-maritime Engineering*, volume 162, pages 155–164. Thomas Telford Ltd, 2009.

[6] Richard Courant. On the partial difference equations of mathematical physics. *Mathematische annalen*, 100:32–74, 1928.

[7] Gary D. Egbert and Svetlana Y. Erofeeva. Efficient inverse modeling of barotropic ocean tides. *Journal of Atmospheric and Oceanic Technology*, 19(2):183 – 204, 2002. doi: 10.1175/1520-0426(2002)019<0183:EIMOBO>2.0.CO;2.

[8] J.P. Frau. Tidal energy: promising projects: La rance, a successful industrial-scale experiment. *IEEE Transactions on Energy Conversion*, 8(3):552–558, 1993. doi: 10.1109/60.257073.

[9] Robert Hagen, Andreas Plüß, Leon Jänicke, Janina Freund, Jürgen Jensen, and Frank Kösters. A combined modeling and measurement approach to assess the nodal tide modulation in the north sea. *Journal of Geophysical Research: Oceans*, 126(3):e2020JC016364, 2021.

[10] Hans Hersbach, Bill Bell, Paul Berrisford, Shoji Hirahara, András Horányi, Joaquín Muñoz-Sabater, Julien Nicolas, Carole Peubey, Raluca Radu, Dinand Schepers, Adrian Simmons, Cornel Soci, Saleh Abdalla, Xavier Abellan, Gianpaolo Balsamo, Peter Bechtold, Gionata Biavati, Jean Bidlot, Massimo Bonavita, Giovanna De Chiara, Per Dahlgren, Dick Dee, Michail Diamantakis, Rossana Dragani, Johannes Flemming, Richard Forbes, Manuel Fuentes, Alan Geer, Leo Haimberger, Sean Healy, Robin J. Hogan, Elías Hólm, Marta Janisková, Sarah Keeley, Patrick Laloyaux, Philippe Lopez, Cristina Lupu, Gabor Radnoti, Patricia de Rosnay, Iryna Rozum, Freja Vamborg, Sebastien Villaume, and Jean-Noël Thépaut. The ERA5 global reanalysis. *Quarterly Journal of the Royal Meteorological Society*, 146:1999–2049, 2020. doi: 10.1002/qj.3803.

[11] Magnus R Hestenes and Eduard Stiefel. Methods of conjugate gradients for solving. *Journal of research of the National Bureau of Standards*, 49(6):409, 1952.

[12] Long Jiang, Theo Gerkema, Déborah Idier, Aimée Slangen, and Karline Soetaert. Effects of sea-level rise on tides and sediment dynamics in a dutch tidal bay. *Ocean Science*, 16(2):307–321, 2020.

[13] T. Kärnä, S. C. Kramer, L. Mitchell, D. A. Ham, M. D. Piggott, and A. M. Baptista. Thetis coastal ocean model: discontinuous galerkin discretization for the three-dimensional hydrostatic equations. *Geoscientific Model Development*, 11(11):4359–4382, 2018. doi: 10.5194/gmd-11-4359-2018. URL https://gmd.copernicus.org/articles/11/4359/2018/.

[14] Tuomas Kärnä, Joseph G Wallwork, and Stephan C Kramer. Adjoint-based optimization of a regional water elevation model. *arXiv preprint arXiv:2205.01343*, 2022.

[15] Jonathan Lambrechts, Richard Comblen, Vincent Legat, Christophe Geuzaine, and Jean-François Remacle. Multiscale mesh generation on the sphere. *Ocean Dynamics*, 58(5):461–473, 2008.

[16] Peter Mooney, Marco Minghini, et al. A review of openstreetmap data. 2017.

[17] Holly E Pelling, JA Mattias Green, and Sophie L Ward. Modelling tides and sea-level rise: To flood or not to flood. *Ocean Modelling*, 63:21–29, 2013.

[18] Lucia Pineau-Guillou. Previmer. validation des atlas de composantes harmoniques de hauteurs et courants de marée. 2013.

[19] Florian Rathgeber, David A. Ham, Lawrence Mitchell, Michael Lange, Fabio Luporini, Andrew T.T. McRae, Gheorghe-Teodor Bercea, Graham R Markall, and Paul HJ Kelly. Firedrake: automating the finite element method by composing abstractions. *ACM Transactions on Mathematical Software (TOMS)*, 43 (3):1–27, 2016.

[20] LP Sha and JH Van den Berg. Variation in ebb-tidal delta geometry along the coast of the netherlands and the german bight. *Journal of Coastal Research*, pages 730–746, 1993.

[21] LP Shah and PL De Boer. Ebb-tidal delta deposits along the west frisian islands (the netherlands): processes, facies architecture and preservation. 1991.

[22] Copernicus Marine In Situ Tac Data Management Team. Product user manual for multiparameter copernicus in situ tac (pum). Report (technical document (specification, manual)), Copernicus Marine environment monitoring service, 2021.

[23] Schmitt Thierry, Schaap Dick, Spoelstra George, Loubrieu Benoit, and Poncelet Cyrille. Emodnet bathymetry a compilation of bathymetric data in the european waters. In *OCEANS 2019-Marseille*, pages 1–7. IEEE, 2019.

[24] Daan Wesselman, Renske de Winter, Anita Engelstad, Robert McCall, Ap van Dongeren, Piet Hoekstra, Albert Oost, and Maarten van der Vegt. The effect of tides and storms on the sediment transport across a dutch barrier island. *Earth Surface Processes and Landforms*, 43(3):579–592, 2018.